Geophysical Prospecting

Geophysical Prospecting

ORIGINAL ARTICLE OPEN ACCESS

Case Study of Dual-Signal Processing of DAS-VSP Vibrator Data From a 3D Survey in a Geothermal Reservoir

Flavio Poletto[1] | Cinzia Bellezza[1] | Gualtiero Böhm[1] | Fabio Meneghini[1] | Athena Chalari[2] | Anna Stork[2] | Mahmut Parlaktuna[3] | Erdinç Şentürk[4] | Deyan Draganov[5] | Gijs van Otten[6] | Sevket Durucan[7]

[1]Istituto Nazionale di Oceanografia e di Geofisica Sperimentale (OGS), Sgonico (Trieste), Italy | [2]Silixa Ltd., Elstree, UK | [3]Department of Petroleum and Natural Gas Engineering, Middle East Technical University, Ankara, Türkiye | [4]Zorlu Enerji Elektrik Üretim AŞ, Şişli, Istanbul, Türkiye | [5]Department of Geoscience & Engineering, Faculty of Civil Engineering and Geosciences, TU Delft, Delft, The Netherlands | [6]Seismic Mechatronics, Veldhoven, The Netherlands | [7]Department of Earth Science and Engineering, Royal School of Mines, Imperial College London, London SW7, UK

Correspondence: Flavio Poletto (fpoletto@ogs.it)

Received: 18 April 2025 | **Accepted:** 13 August 2025

Funding: The SUCCEED project is funded through the ACT programme (Accelerating CCS Technologies, Horizon 2020 Project No 294766). Financial contributions made by the Department for Business, Energy & Industrial Strategy UK (BEIS), the Ministry of Economic Affairs and Climate Policy, the Netherlands, the Scientific and Technological Research Council of Turkey (TUBITAK), Orkuveita Reykjavíkur Iceland/Reykjavik Energy (OR) and the Istituto Nazionale di Oceanografia e di Geofisica Sperimentale (OGS), Italy, are gratefully acknowledged.

Keywords: distributed acoustic sensing | dual signals | geothermal reservoir | three-dimensional vertical seismic profile | vibrator source

ABSTRACT

The three-dimensional (3D) distributed acoustic sensing (DAS) vertical seismic profile (VSP) technique is an effective tool to characterize subsurface reservoirs, enabling the use of large and densely sampled borehole receiver arrays with many surface vibrator source points for onshore time-lapse monitoring. However, the processing of the DAS VSP signals for imaging purposes is based on a reliable wavefield separation, which may depend on the recognition and quality of the direct arrivals. To overcome this limitation for common-source gathers with poor signal-to- noise ratio or with interferences, we apply the dual-signal processing method, which allows us to estimate and separate the DAS wavefields by signals' combination without arrival picking. We present a case study of a 3D VSP DAS dataset recorded at a geothermal reservoir in Turkey, showing that the method, similar to a geophone and hydrophone combination, is robust and effective and can be advantageously integrated with the conventional processing. Supported by signal benchmarking, modelling and signal-to-noise ratio analysis, we treat common-source and common-receiver data. Our analysis shows the advantages and limitations of the proposed approach, valuable in the time-lapse perspective.

1 | Introduction

It is nowadays accepted that the use of three-dimensional (3D) DAS (distributed acoustic sensing) VSP (vertical seismic profile) technology provides an additional support during exploration and development activities and an effective tool to characterize subsurface reservoirs (Zwartjes et al. 2018; Liborio et al. 2023), including four-dimensional (4D) monitoring in ongoing production wells (Ali et al. 2021). In fact, 3D DAS VSP enables utilizing large and densely sampled borehole receiver arrays with many surface vibrator sources for time-lapse injection monitoring applications. To demonstrate continuous active seismic monitoring for onshore applications, Correa et al. (2021) used DAS downhole permanent installations in boreholes and orbital vibrator surface sources. They evaluated the results of DAS VSP data for CO_2 injection monitoring in test wells. The processing of data for

seismic characterization and imaging seismic reflections involves the key step of wavefield separation. Beyond separation methods using multichannel dip filters, such as Tau-P transform and frequency-wavenumber (FK) filtering (Yu et al. 2023; Ali et al. 2021), the common VSP approach uses the first breaks as key information, with results that may depend on the recognizability and quality of the direct arrivals. To overcome this limitation in the case of complex data, such as those with large offsets and problematic seismic responses, we use the dual-signal approach (Poletto et al. 2016). The dual-signal method provides a powerful tool based on physical insight. In this work, we present the results of the dual-signal processing approach with DAS signals. This method enables the estimation and separation of propagated wavefields at a recording position without detailed signal interpretation and direct arrival picking (Poletto et al. 2016, 2023). Compared to multichannel methods, this method is essentially a variant of a single-trace processing approach. The corresponding dual signal is obtained by processing the native DAS signal, that is, the output signal from the DAS system, and together with the native signal they form a dual-signal pair. Their nature is discussed in the Theory section and compared to that of a geophone signal recovered from DAS data (Sayed et al. 2020; Soulas et al. 2023). The dual signals contain wavefields with concordant- and opposite-sign components. Once the dual signal is calculated from the native one, similar to geophone and hydrophone combinations (e.g., Loewenthal and Robinson 2000; see also Furre and Eiken 2014), their summation and subtraction performed with estimated optimal scaling factors can be used to separate downgoing (DW) and upgoing (UP) waves, or equivalently, depending on the acquisition geometry, forward- and backward-propagated wavefields. We revise the theory and discuss the parameters and the different approaches usable to calculate the dual wavefields in the borehole DAS receiver-array signals.

We present results of the analysis performed with 3D VSP DAS data of a near-vertical observation well in a geothermal reservoir used to monitor underground injection of carbon dioxide in Turkey (Parlaktuna et al. 2021). The dataset was obtained in the framework of a base study of a time-lapse monitoring project (Durucan et al. 2021). The novel enhanced-sensitivity source–receiver VSP acquisition of this survey, accomplished in the context of a more extended surface-well comprehensive active seismic acquisition layout, is described in the next section. The study presented in this work shows that the adopted dual-signal processing method can be robust and effective in the absence of signal picking and can be advantageously integrated with the conventional VSP-processing approach, providing additional information to calibrate the dual calculation parameters. Sample results obtained with the baseline 3D VSP survey are discussed in the time-lapse perspective, showing advantages and limitations of the proposed processing method. Although in its initial phase of 3D processing, the study covers and highlights several aspects.

The refinement of the scaling combination-factor estimation in a deferred processing phase is one of the aspects evaluated in this work. The estimation of the combination factor is also related to the sensitivity of the dual DAS signals from measurements of waves with different incidence angles and apparent velocities. Benchmarking of the dual DAS VSP results with those of a conventional DAS VSP processing, with the measurements of the signal-to-noise ratio (SNR) in the dual wavefields and of normalized root mean square (NRMS) of their difference confirms the robustness of the dual-signal method. We highlight with examples the differences in the original native and dual signals, using data at different depths recorded with different vibration-point offsets. We investigate the combination options and solutions for different wavefields. The interpretation of the signal's sensitivity in common-receiver data recorded at different depths is supported by 3D ray tracing.

2 | Site Description and Acquisition Layout

We present the approach and the initial quality control (QC) results of a dual-DAS VSP acquired using semi-permanent fibre optic DAS technology during a baseline survey of a CO_2 injection monitoring project in a geothermal production reservoir. The monitoring campaign was performed in the framework of the SUCCEED project (Durucan et al. 2021) and was acquired at the Kizildere site of Zorlu Energy (Turkey), where geothermal fluid is produced from and re-injected into a carbonate reservoir at depths from 500 to 3500 m and 220–245°C reservoir temperature (Parlaktuna et al. 2021) (Figure 1). We used a joint configuration of helically wound fibre optic cables installed on the surface in shallow trenches and two instrumented wells with downhole high-sensitivity engineered fibre. A dense spatial sampling approximately every 1 m in depth was recorded with a time sampling interval of 1 ms. The fibre, with a 10-m gauge length, was lowered using a semi-permanent cable suspended in the vertical cased wells. These wells are two observation wells, R-3 and KD9, shown in Figure 2. In this work, we present the VSP results obtained with the high-sensitivity measurements in well R-3, where a linear engineered fibre was co-located together with a conventional DAS fibre. The depth of the observation line in the well is approximately 940 m.

The fibre optic arrays in the wells recorded one single-offset VSP dataset for each DAS line in each well, namely R-3 and KD9, for every shooting position. The source was a novel electric seismic vibrator (for more details, see Meneghini et al. 2024) with 10 kN total force, operated on the surface with a 3D arrangement of vibration points (VPs) along accessible paths in the proximity of and around of the wells and along the surface DAS sensors lines, supported with bi-axial geophone measurements (Figure 2). The seismic source was used in a vertical-vibration mode.

After QC tests performed in the startup phase, in which we recorded calibration VSPs with 24 vibrations per VP, we used a recording length of 20 s, a sweep length of 15 s, six vibrations per VP for the vertical stack of the cross-correlated data with the vibrator source signal obtained using upsweeps with frequency 4–160 Hz.

These values were considered a satisfactory compromise to record data of good quality using a large number of 3D vibration positions to seismically illuminate the reservoir, within the limits of the operational resources. The VP array (Figure 2) was determined after subsurface illumination analysis, using existing Petrel models of the reservoir (Figure 1) to define the seismic model in the pre-survey feasibility study (Parlaktuna et al. 2021) (Figure 3). The focus of the study is on the reflections from the

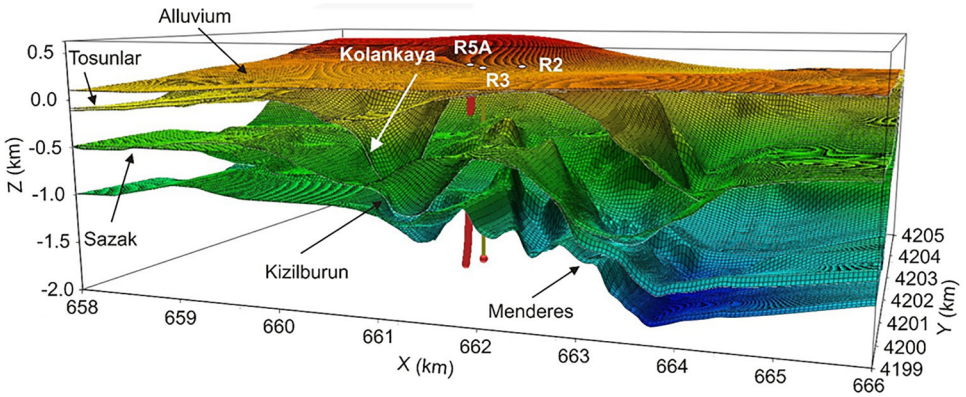

Figure 1 | Initial reservoir model, showing the complex structural setting of the investigated zone. The horizon of the reservoir at Menderes is the deeper one.

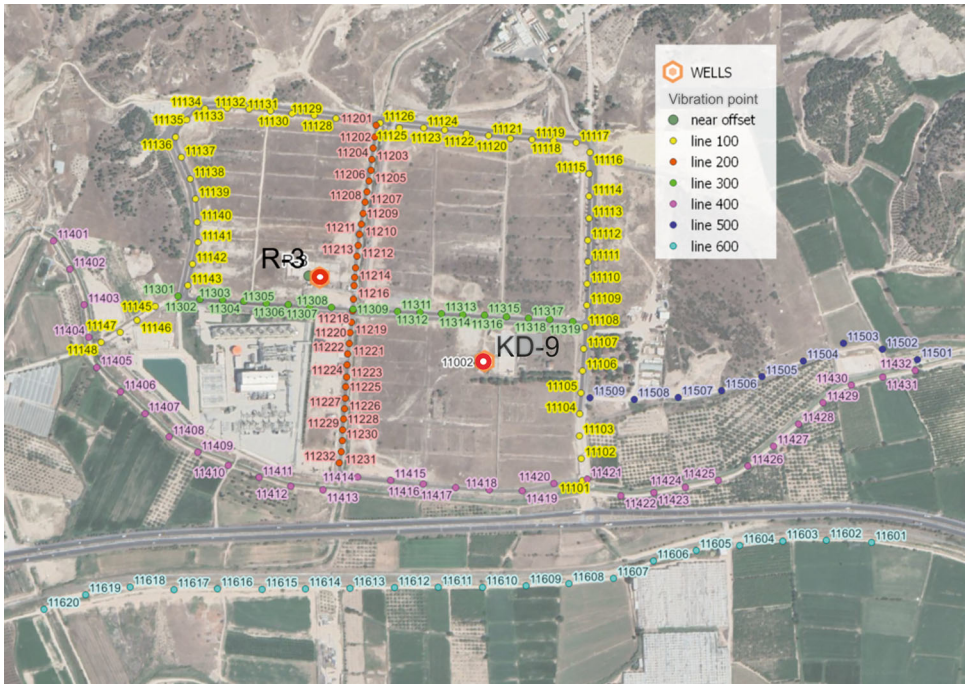

Figure 2 | Field acquisition layout with vibration point positions around wells and along the surface seismic lines. We used the signals recorded in well R-3.

reservoir at the top of the Menderes Metamorphics formation (Parlaktuna et al. 2021), which is the deepest horizon in Figure 1. Another, shallower, reservoir is the Sazak formation.

Ray-tracing analysis of wave paths in the dipping formations showed that the concentration of the reflection zones of interest on Menderes is up-dip, north-oriented, relative to the wells where the DAS VSP data were acquired, from surface to depth of 939 m below ground level (b.g.l.) (Chalari et al. 2023). Hereafter, in the paper, all the depths are intended as depths b.g.l. The total number of VPs surrounding the wells was 162, with a maximum offset of approximately 1100 m. The interval of the shooting positions was variable, with intervals ranging from 20 to 80 m along the surface-receiver lines and around the wells, along paths constrained by logistic and environmental conditions. Because of the accessibility restrictions, it was not possible to adopt a more regular 3D shooting geometry, as, for example, a two-dimensional (2D) regular grid (Ali et al. 2021) or a spiral grid around the DAS-instrumented wells (Martuganova et al. 2022). In Figure 2, the shooting-line branches are marked by different colours. The source interval along the north-south line 200 was 20 m and larger for the other lines.

Quick-look VSP results were obtained during the initial QC performed in-field and remotely, as well as from the prompt processing of the data few days after the survey acquisition. Tuning of the acquisition parameters performed during the QC phase allowed us to obtain a good-quality signal, subsequently used for wavefield processing. The VSP data processing takes advantage of the dual-field separation method, applied effectively with the fibre optic data, gaining from their dense and regular spatial sampling with receivers in the wells (Poletto et al. 2016).

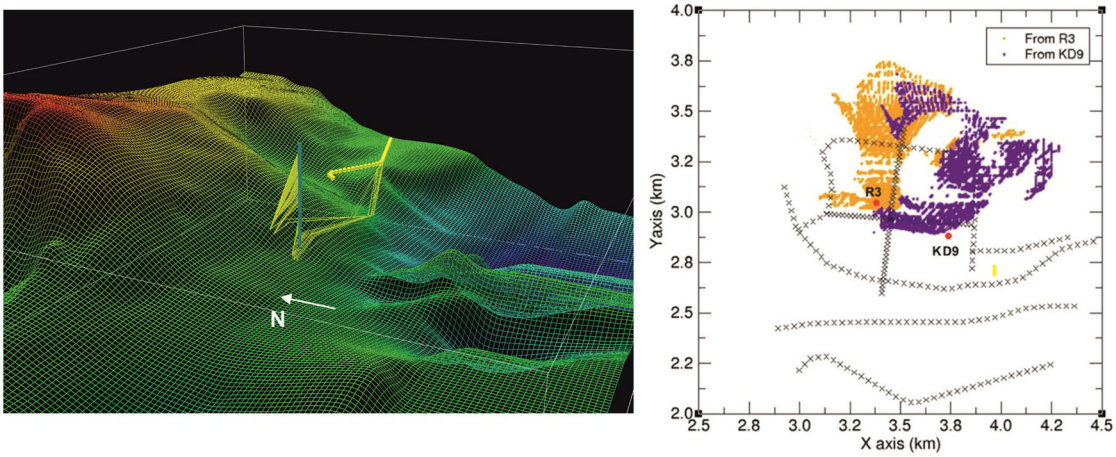

Figure 3 | Reservoir illumination by VSP reflections on the top of Menderes. (a) Up-dip reflections recorded in the well R-3 using the selected surface source line marked by yellow dots. (b) Analysis of illumination obtained using wells R-3 and KD-9. The black crosses denote the 3D areal surface-source positions around the wells.

This approach enabled separating UP and DW waves in the VSP wavefields. This method does not require first-arrival picking, typically needed for conventional VSP. This is an advantage for the extensive processing of data acquired with 3D configurations. During the early phase of the campaign, we tested the dual-signal separation method on a sample of near-offset VSPs that allowed a prompt update for calibration and interpretation of the subsurface model.

3 | Theory and Method

The signals used for dual-field processing are the native DAS output and a signal directly calculated from the native DAS output, which as a standard provides one single component for each trace position. Let u be the axial displacement along the cable. The native fibre optic signal s obtained at the cable position z is typically the strain rate

$$s(t,z) = \frac{\partial}{\partial t}\frac{\partial u(z,t)}{\partial z}, \tag{1}$$

or the strain

$$\varepsilon(t,z) = \frac{\partial u(z,t)}{\partial z}, \tag{2}$$

where z is the cable axial coordinate and t is time. The corresponding dual signals are particle acceleration and particle velocity, calculated by

$$a(t,z) = \frac{\partial}{\partial t}\int^{z} s(z',t)dz', \tag{3}$$

and

$$v(t,z) = \frac{\partial}{\partial t}\int^{z} \varepsilon(z',t)dz', \tag{4}$$

respectively. One may argue that a direct calculation of the particle velocity signal to recover the corresponding geophone signal can be done using the space integration of the strain rate (1), as (e.g., Willis, 2022)

$$v(t,z) = \int^{z} s(z',t)dz'. \tag{5}$$

This calculation (Equation 5) may be conveniently used, for example, for DAS signal and noise analysis by a comparison with the geophone signal (Soulas et al. 2023). However, the velocity signal provided by (5) or (4) is not the dual signal of the strain rate (1). When the native signal $s(z,t)$ is the strain rate, its dual signal is the particle acceleration $a(z,t)$. When the native output is the strain $\varepsilon(z,t)$, its dual signal is the particle velocity $v(z,t)$. In fact, these quantities, apart from polarity variations, contain wavelets with the same signature within a dual-signal pair. Conveniently, for DAS VSP data, we choose the representations with the dual pairs composed of the strain rate and the particle acceleration with opposite polarity, or the strain and the particle velocity with opposite polarity, depending on the nature of the native DAS signal. In the following, neglecting the distinctions made for the physical nature of the native DAS signals (for a similar discussion on dual signals of different physical quantities in drill pipes, see also Poletto et al. 2004), without loss of generality, for convenience, we use a unique general formal notation for the dual quantities. In all the following examples, we will denote the native signal as $s(z,t)$ and its dual signal as $v(z,t)$, intending that they may have a different physical meaning. The use of dual strain and particle velocity signals may be more convenient when we compare DAS signals with those of particle velocity transducers (geophones), similar to the procedure used with geophone and hydrophone data. As shown by Poletto et al. (2016), the use of strain rate and acceleration is effective for dual-signal processing.

3.1 | Integration Limits

From a computational point of view, the spatial integration provides an effective and robust approach to calculate the dual wavefields of signals that are a superposition of DW and UP waves. The calculation is easy and effective. Different computational approaches can be used for the spatial integration of pilot-sweep cross-correlated data (Willis 2022). Assume a single-offset VSP recorded at depths z, with $z_1 \le z \le z_2$, sorted with the shallower traces on the left side and the deeper traces on the right side of the common-source gather. Using the definite integral for dual-signal calculation gives

$$v(z,t) = -\frac{\partial}{\partial t}\int_{z_1}^{z} s(z',t)dz' + v(z_1,t) = -I_L(z,t) + v(z_1,t), \quad (6)$$

that we define as the left-to-right (LTR) approach to calculate $v(z,t)$. The quantity $v(z_1,t)$ can be regarded as an integration constant in depth, which has to be compensated in the processing phase, due to the fact that on the left side of z_1 we do not have data, or equivalently, we do not have data to know the dual signal at z_1. Assuming a plane-wave approximation, this introduces a flat noise-like component, constant with depth z. In realistic cases, in the presence of signal amplitude variations due to changes in the recording conditions, the integration may cause local "brushstroke" effects. Moreover, the integration constant may be affected by shallow-well local noise of high amplitude and may include other constant versus depth (or axial coordinate) noise components, such as the flat optical common-mode noise (CMN) (Willis, 2022), filtered by the cross-correlations. In fact, a single-offset VSP dataset obtained at a VP position is a common-source gather of traces that, in some cases, can be affected by CMN. A result equivalent to Equation (6) is obtained with the right-to-left (RTL) approach as

$$v(z,t) = -\frac{\partial}{\partial t}\int_{z_2}^{z} s(z',t)dz' + v(z_2,t) = -I_R(z,t) + v(z_2,t), \quad (7)$$

which also gives $v(z,t)$, apart from the different boundary conditions that have to be compensated to clean the signals. Figure 4a shows the uncompensated dual field $[v(z,t) - v(z_1,t)]$ of a near-offset DAS VSP calculated by left-side integration. The presence of the side integration effect with constant events versus depth, starting at the left-side traces, is obvious. These events mask the recovered dual signal from the native DAS VSP (not shown in this figure). Figure 4b shows the same data after removal of the flat side-integration effects by a narrow FK filter that removes the nearly horizontal components, thus providing a cleaned estimation of $v(z,t)$. A narrow strip of residual noise is present at the right-side edge of the gather after the FK-filter application. This local effect, due to the abrupt interruption of VSP data at the maximum depth, can be mitigated with strategies based on data tapering, padding and a combination of LTR and RTL integration approaches. The DAS dual signal recovered in this example is clean, with similar SNR to that of the original one (as in Figure 5a) and becomes clearly observable in Figure 4b.

3.2 | Wavefield Separation

Figure 5a and 5b shows the native $s(z,t)$ and the calculated dual $v(z,t)$ signals, respectively, of a near-offset DAS VSP. The polarity of the dual wave $v(z,t)$ is set to represent the DW waves with the same polarity in Figure 5a,b. These dual signals contain events with the same waveform but opposite polarity, and globally they show similar SNR. The effect of the space integration (Equation 6) used for the calculation of the dual signals is to produce signals with opposite polarity starting from events with the same polarity but opposite slopes. The traces obtained at the same z position in Figure 5a,b contain progressive waves with the same polarity and regressive waves with opposite polarity, that is, the integration causes the reversal of the polarity for the regressive waves in $v(z,t)$ relative to those in $s(z,t)$ (Poletto et al. 2016). This effect is evident for the DW and UP waves of Figure 5. While in Figure 5a,b, we have the same direct arrivals and DW waves in intervals with uniform seismic velocity, the UP reflections have opposite polarity. This effect is highlighted for the selected reflection phases indicated by the red arrows. The pointed phase of the reflection signal in (a) is negative and appears as a white throat, while the corresponding signal in (b) is positive and appears as a black peak. This event is interpreted as a reflection at the interface black between the Kolankaya and the Sazak (Pliocene limestones) formations, with the P-wave velocity variations shown in Figure 6. The Sazak formation is the first and shallower reservoir of the Kizildere geothermal site. The second and deeper reservoir is the Menderes formation (Simsek et al. 2005).

To perform the wavefield separation, dual signals obtained at the same recording position z with the same source are combined by simple trace-by-trace summation and subtraction of the native $s(z,t)$ and dual $v(z,t)$ signals, after a scaling required to adapt the magnitude of the calculated events. Assume, for simplicity, the case of a plane-wave approximation, with wavefronts normal to the optical cable axial direction (axial approximation). Let the native DAS signal be the superposition of progressive and regressive waves travelling in the axial direction with propagation velocity $\pm c$. We calculate the dual-signal combinations at depth z as

$$DW(z,t) = 0.5\left[s(z,t) + \frac{1}{c}v(z,t)\right], \quad (8)$$

and

$$UP(z,t) = 0.5\left[s(z,t) - \frac{1}{c}v(z,t)\right], \quad (9)$$

where the scaling factor $\pm 1/c$ is the slowness of the signals (Daley et al. 2016; Poletto et al. 2016). The polarity of the UP signal (9) is that of the UP waves in the native signal. When, as usual, we have seismic signals containing more waves with different propagation velocities, say, different body waves, like P-waves and S-waves, as well as borehole wave modes and noise in the well, in a more general form, Equations (8) and (9) may be reformulated as

$$DW(z,t) = 0.5[s(z,t) + \alpha v(z,t)], \quad (10)$$

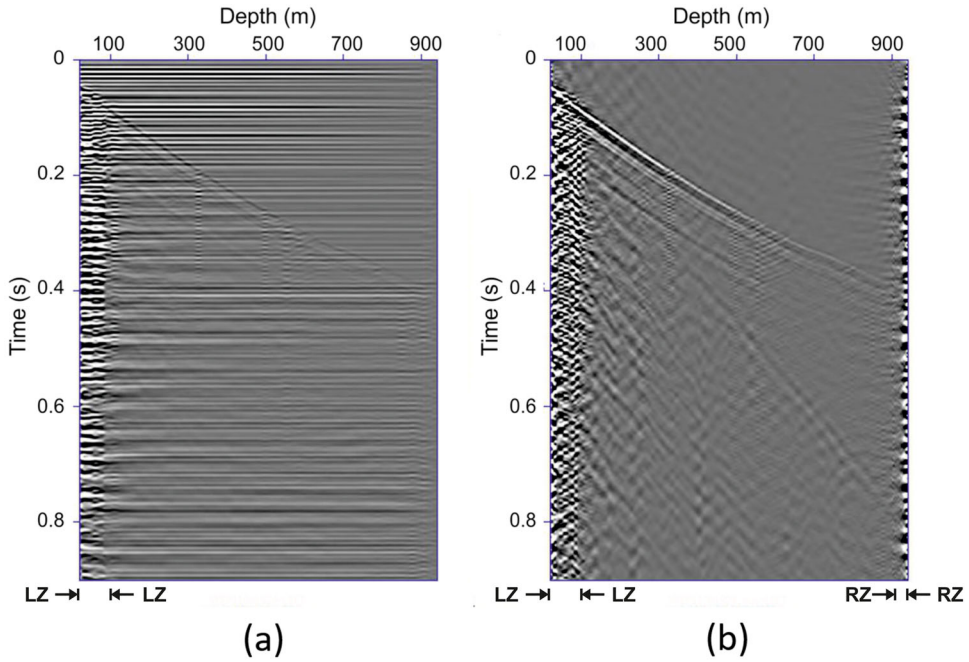

Figure 4 | (a) Dual signal of a near-offset DAS VSP obtained with LTR estimation. (b) Dual signal of a near-offset DAS VSP after side-integration effects removal. At the bottom of the figures, two margin zones are indicated by arrows. The left-side zone (LZ), with a width of approximately 80 traces, indicates the shallower interval of traces more affected by borehole noise with large amplitude. However, this type of noise is already present before integration, as it can be seen in the native signal in Figure 5a. Conversely, the right-side zone (RZ), with a width of approximately 35 traces, shows more clearly near-edge distortions introduced by the narrow FK filter used to remove the horizontal side-integration noise.

and

$$UP(z,t) = 0.5[s(z,t) - \alpha v(z,t)], \tag{11}$$

respectively, where α is the combination coefficient, which, we consider, may depend also on cable coupling conditions. If the medium is not uniform $\alpha = \alpha(z)$. Therefore, with the superposition of different waves, α becomes a suitable value to focus a desired component, for example, or a reasonable averaged value for quick wavefield interpretation. In some particular cases, it might be convenient to use different values of α for direct and reflected waves. Conversely, the estimation of the dual signal $v(z,t)$ is not determined by the choice of the scaling factor, as it depends only on the data integration. In the previous equations, two domains, one of the native signal $s(z,t)$ and one of the dual signal $v(z,t)$, are used for the combination. Although for VSP purposes, the dual velocity signal is the preferred one for comparison with surface seismic results from geophones (Sayed et al. 2020), in Equations (10) and (11), we have selected the native signal as the reference one to estimate the combination coefficients to better evaluate the processing effects relative to the native DAS output signal. With $c = c(z)$ or equivalently $\alpha = \alpha(z)$, similar separated results can be calculated using the combinations

$$0.5[c(z)s(z,t) \pm v(z,t)], \quad \text{or} \quad 0.5[s(z,t)/\alpha(z) \pm v(z,t)], \tag{12}$$

to obtain DW and UP waves shaped using the dual signal $v(z,t)$ as the reference total wavefield.

3.3 | Discrete Signal Representation

When dealing with discrete signals, the progressive sum of the traces can be used to estimate the space integral, for example, by

$$I_L(z_i,t_j) = \sum_{z_k=z_1}^{z_i} s(z_k,t_j)\Delta z_k, \tag{13}$$

with $z_1 \le z_k \le z_i$ and $z_1 \le z_i \le z_2$, where z_k are the discrete receiver depths, t_j the discrete times and $\Delta z_k = z_{k+1} - z_k$ are the receiver intervals. From a practical point of view, the detailed knowledge of the variable Δz_k between receivers could be an issue for wireline borehole data recorded using short arrays. For signals sampled using arrays with receiver interval Δz, as it normally occurs for DAS arrays, the integral (13) becomes

$$I_L(z_i,t_j) = \Delta z \sum_{z_k=z_1}^{z_i} s(z_k,t_j), \tag{14}$$

which gives the integral as a scaled progressive summation of traces and the combination factor for the progressive summation becomes $\alpha = \Delta z/c$ to take into account the relative receiver distance.

4 | Wavefield Processing of Real Data

The dual-processing method provides an effective separation of DW and UP signals in DAS VSP data. The approach does not require the picking of the direct arrivals, which, conversely, is

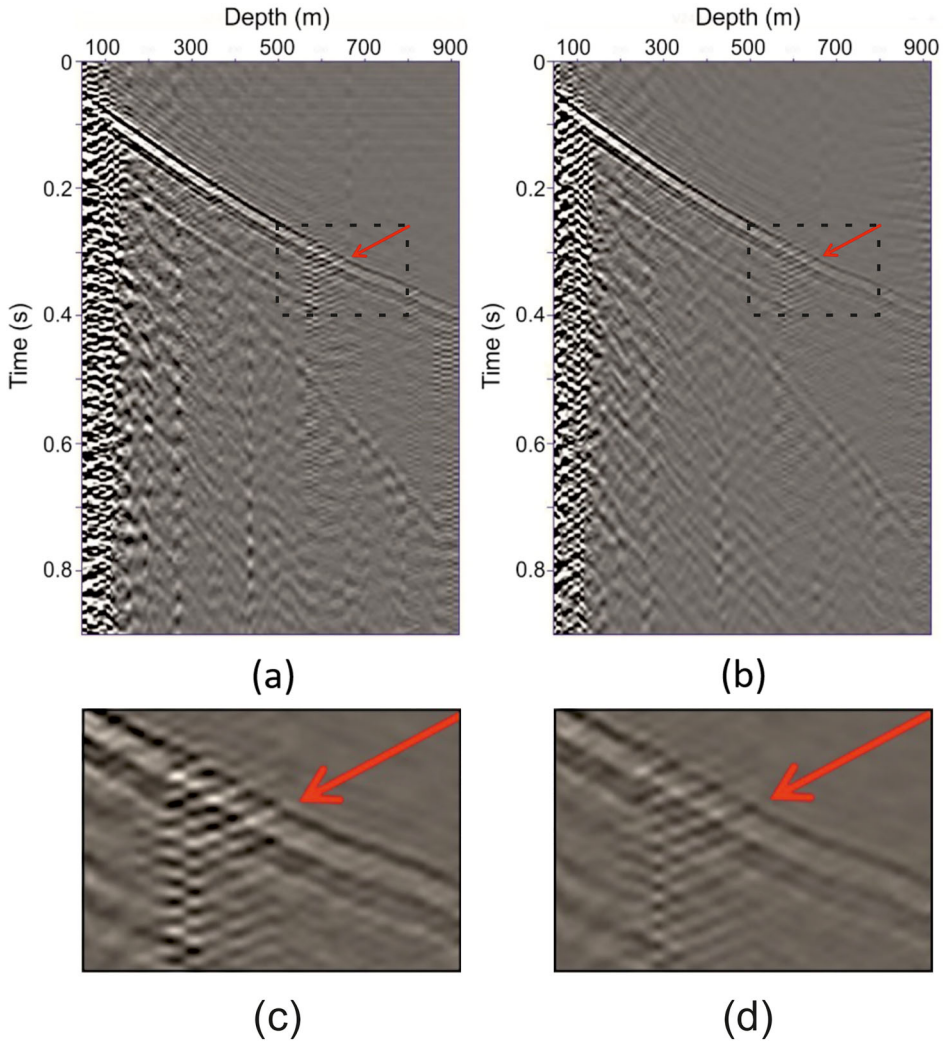

Figure 5 | (a) Native DAS signal. (b) Calculated DUAL signal. Direct and downgoing waves have the same polarity in (a) and (b). Upgoing reflections have opposite polarity in (a) and (b), as indicated by the red arrows at approximately 645 m depth. Panels (c) and (d) show enlargements of the parts enclosed by the dashed rectangles in (a) and (b), respectively.

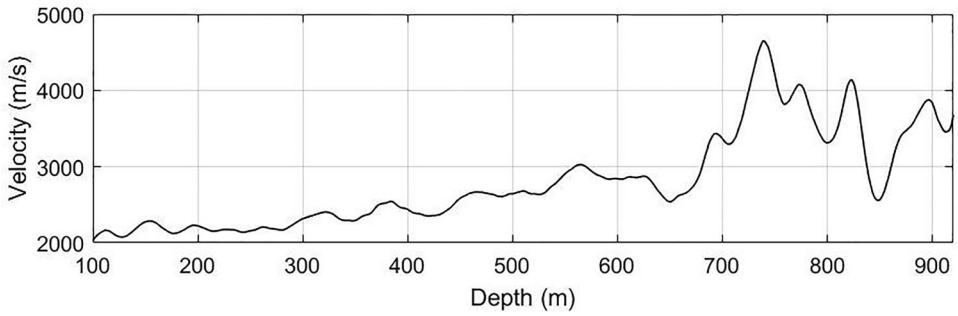

Figure 6 | Vertical P-wave velocity profile in well R-3 obtained from the picking of the first breaks in the dual downgoing separated data. The changes in the velocity at about 650 m depth correspond to the transitions at the top of the Sazak formation.

a crucial step in conventional VSP processing. However, the additional use of direct signal picking is obviously beneficial. Depending on the data quality, dual-signal processing makes it possible to quickly identify UP reflection fields for look-ahead prediction and reflectivity characterization in the well. This information is important, especially when conventional borehole seismic data are not available for calibration of the initial seismic model. In the analysis of the results, we take into account that a moving-window space averaging effect is included in the DAS data recorded regularly every metre with a gauge length of 10 m. A gauge moving-filter (e.g., Sayed et al. 2020; Willis 2022) prevents from aliasing, and with a value of 10 m

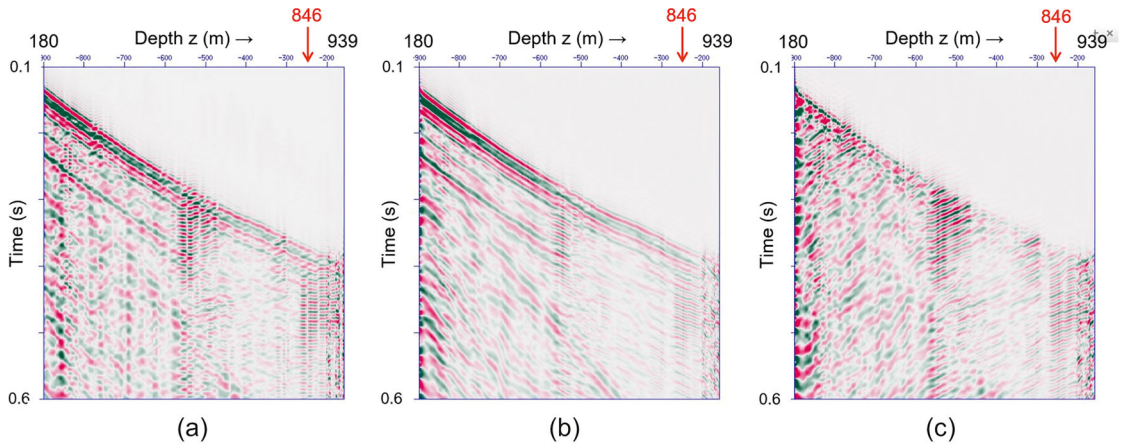

Figure 7 | Sum and subtraction of DAS VSP dual fields. (a) Total field (native), (b) downgoing wavefields and (c) upgoing wavefields. The total wavefield (a) includes the downgoing direct arrivals and the upgoing reflections. The downgoing wavefield (b) contains the separated downgoing events. The upgoing wavefield (c) provides a good representation of the upgoing reflections. The red arrows indicate the positions of the trace selected for the Fourier frequency analysis (Figure 8) in each panel.

gauge lenght, receiver intervals larger than 1 m can be considered suitable for the dual-signal calculation method, with results showing small differences mainly at higher frequencies. We applied this analysis to the pilot-correlated field data acquired at Kizildere.

After initial QC at a few selected VPs, the survey was performed by stacking six cross-correlations at each VP. This was considered a suitable compromise in the economy of the project. This limitation is considered in the processing phase and discussed with the analysis of the weaker, deeper and offset DAS VSP data.

4.1 | Common-Source Results

Figure 7 shows the quality of the DAS VSP dual-signal processing for a near-offset VSP together with the wavefield separation results. These results were obtained by processing the data of the DAS cable of a QC test acquired with the stack of 24 records at the same source position. Figure 7a shows the native field before separation, that is, the original total field versus depth. Figure 7b and 7c shows the calculated DW and UP fields, respectively. It is noteworthy that these results were obtained simply by scaling the dual signals using an estimated constant α factor and by combining, that is, summing and subtracting, the dual signals after scaling. The separation of the DW and UP events is effective, and the wavefields are clean. To verify the quality of the frequency content for the deeper seismic signals, the Fourier frequency spectra of single traces selected at 846 m depth from each panel of Figure 7 are shown in Figure 8. They show that the signal bandwidth ranges between approximately 10 and 120 Hz. In an early phase during acquisition, and by prompt processing after acquisition, the dual-processing method was used to quickly interpret the seismic reflections, in particular the interpreted reflection from the Menderes reservoir, and the data used to update the velocity model of the site. The initial model was obtained from the geological Petrel model of Figure 1, initially calibrated with indicative velocities estimated, in the absence of available borehole-seismic information, with the support of laboratory data evaluated prior to the seismic survey (similar to Janssen et al. 2021). Figure 9 shows an example of early results produced for this purpose, where the discrepancies between the pre-survey and the during- and after-survey seismic times and velocities are verified for the Menderes horizon.

4.2 | Comparison of Dual-Signal With Conventional VSP-Processing Methods

To benchmark the dual-signal method, we process the near-offset DAS VSP acquired with the stack of 24 vibrations during the QC phase. The separation of the dual wavefields is calculated by tuning the variable combination coefficients along the profile to improve the results. More details of this approach are discussed later in this paper. As a conventional VSP processing method, we choose a median filter after picking of the first arrivals. We use a 31-trace median filter to approximate the DW wavefield, which is then subtracted from the total field to obtain the residual field with the UP signals. Figure 10a,b,c shows the separated DW signals obtained from the dual-signal method, the median filter and their difference, respectively. Figure 10d,e,f shows the corresponding UP signals. In both the differences in Figure 10c,f, we observe the effectiveness of the removal of the coherent events, with some variability due to different noise conditions and the nature of the residual coherent events related to the choice of the processing parameters in the two methods. In fact, we do not expect that the two different methods focus on the same events. The dual-signal method is driven by the choice of the combination coefficients, while the median-filter method depends on the picking of the direct arrivals and the choice of the number of filter points. The starting native DAS and calculated dual DAS signals have similar SNR. Figure 11a shows as an example of the SNR of the native and dual total fields in a depth window between 380 and 500 m. In both total fields, the SNR values are obtained as the ratio of the root mean square (RMS) values that were calculated in a short time window centred around the direct arrivals and in a time window before the direct arrivals. This comparison ensures that we sum and

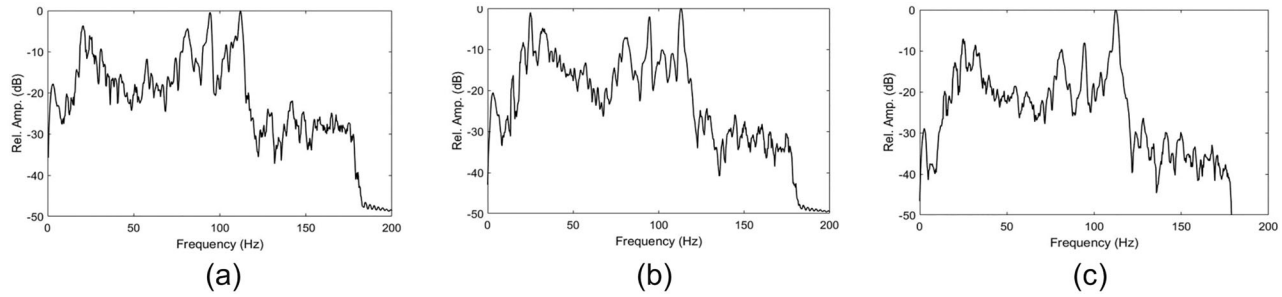

Figure 8 | Fourier frequency spectra of the (a) total field (native), (b) downgoing waves and (c) upgoing waves shown in Figure 7, calculated for the traces at depth 846 m in R-3, as indicated by the arrows in Figure 7.

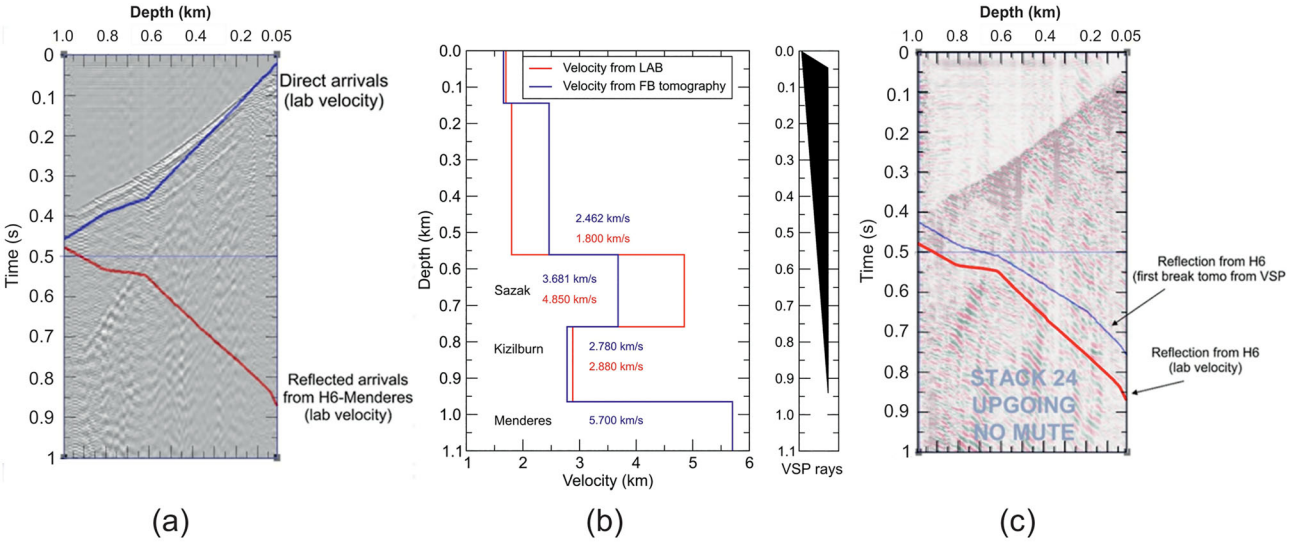

Figure 9 | Example of early DAS-VSP results produced for prompt QC purposes, and used to update the velocity model of the reservoir. (a) Comparison of DAS VSP data with direct (blue line) and reflection (red line) arrivals derived from a pre-survey laboratory model (Janssen et al. 2021). (b) Velocity model update using the DAS VSP results. (c) The upgoing signal from the dual-signal processing is compared with the ray tracing results calculated with the updated model (blue line) and with the presurvey model (red line).

subtract dual signals with similar SNR. If the level of noise in the calculated dual signal were much higher than that of the original one, the combination would have resulted in worse separated traces relative to the native DAS signal. To quantify the consistency and repeatability of the results obtained with the dual-signal and median-filter processing methods, we calculate the NRMS norm (Kragh and Christie 2002) in the DW and UP differences shown in Figure 10c and 10f, respectively. Figure 11b shows the NRMS of the DW and UP signals in the same depth interval as shown in Figure 11a. The NRMS of the DW signal is low, around 25%, denoting an appreciable matching of the data obtained with the different processing methods. The DW NRMS is lower, about half, of the UP one, because the DW signal is more energetic than the UP one relative to the residual noise after wavefield's separation. Figure 12 shows in more detail the differences in the UP signals of Figure 10 with enlarged plots. The UP signals obtained by the dual-processing method (panels a and c) generally have a better quality than the signals obtained by the median-filter processing method (panels b and d), which is based on the subtraction of the estimated DW signals aligned with the direct arrivals. This is particularly evident in the panels at lower frequencies (c and d), where a lowpass filter (4, 8, 50, 60 Hz) was applied. Arrows indicate relevant reflections in the reservoir zone close to the total well depth. We quantify the frequency dependence of the reflection signals by calculating the corridor stack (CS) (Hardage 1983) of the muted two-way-time (TWT) UP signals. Figure 13a and 13b shows the TWT reflections obtained by dual and median filter methods, respectively. The reflections are aligned by adding the same first-break times picked on the direct arrivals. We observe a generally good agreement between results (a) and (b), but we can also see improvements in the continuity of the dual signal (a). From each panel, we obtain one CS trace as a reliable estimation of the DAS VSP reflection signal. The CS traces in the time domain are not shown here. The frequency contents of the CS signals are compared in Figure 13c, which shows the amplitude curves (dB) smoothed in frequency using a 15-Hz window. The curves have different slopes. Their trends are similar, with comparable amplitudes at high frequencies, but they differ at lower frequencies, where the amplitude of the median result is about 7–8 dB lower than the amplitude of the dual result. This comparison confirms the advantage of the dual-signal processing method over the median-filter separation method for the separation of reflection signals with improved low-frequency content.

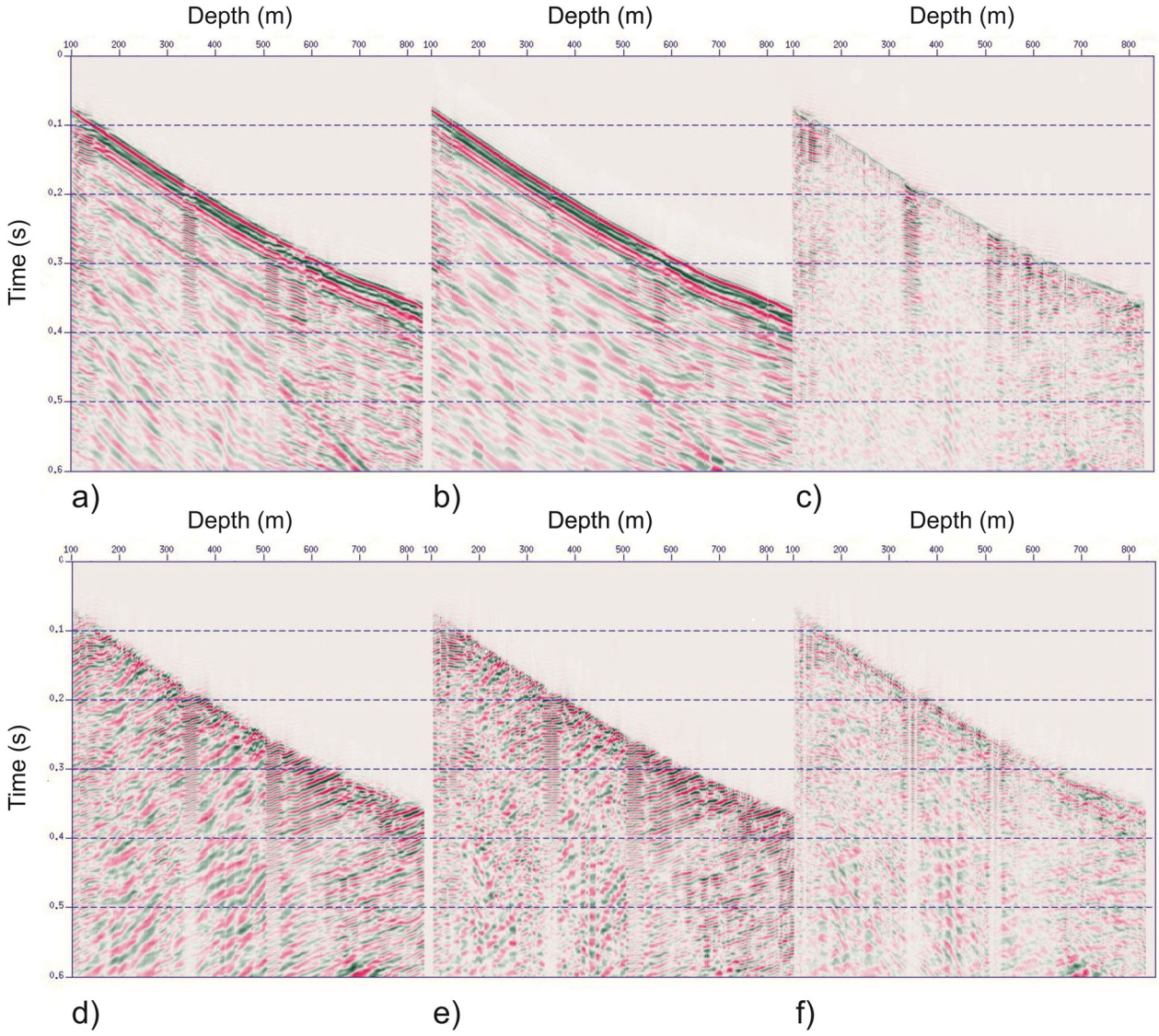

Figure 10 | Downgoing wavefield calculated using (a) the dual-signal processing approach and (b) the median filter. In (a), the dual signal used for the separation at the depth z is calculated by summation of the native traces in the variable-length interval of integration spanning from the first trace at z_1 to the trace at z (Equation 14). In (b), we used a moving median filter with a fixed length of 31 traces spaced 1 m to separate the wavefields. (c) The difference of the results in (a) and (b). Figure 10d,e,f shows the corresponding upgoing wavefields, respectively.

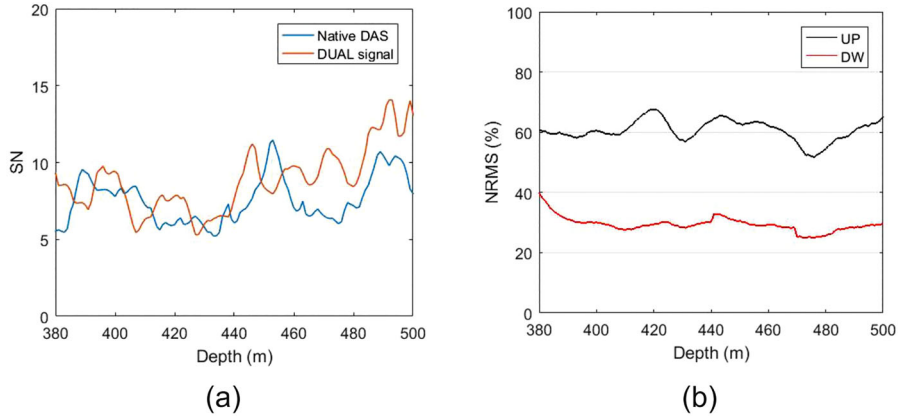

Figure 11 | (a) Example of SNR of the native DAS signal (blue line) and of the dual DAS signal before wavefield separation. (b) Example of NRMS of the upgoing (blue line) and downgoing (red line) differences shown in Figure 10f and 10c signals, respectively.

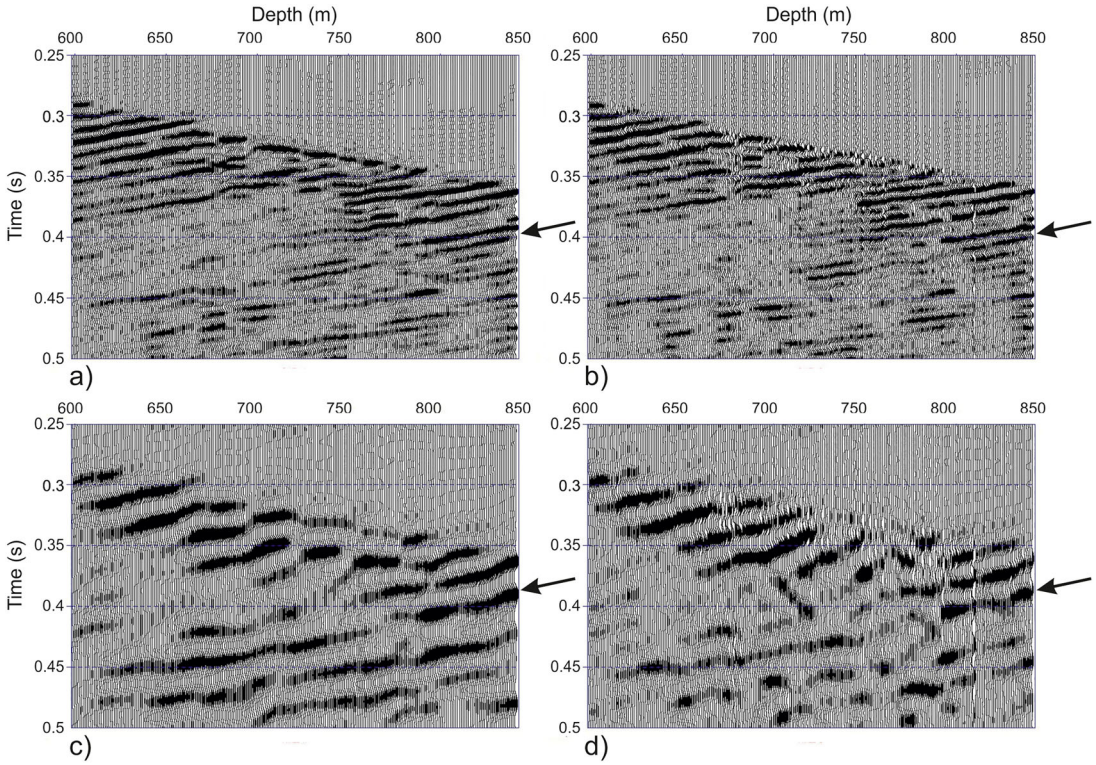

Figure 12 | Zoomed-in sections obtained with the upgoing-dual and upgoing-median data of Figure 10 in the depth interval 600–850 m and in a shorter time window. The seismic signals in the left column (panels a and c) are the upgoing fields obtained by dual-signal separation. The seismic signals in the right column (panels b and d) are the upgoing fields obtained by median-filter separation. The first row at the top (panels a and b) shows the signals without an additional BP filter. The second row (panels c and d) shows the lowpass-filtered (4, 8, 50, 60 Hz) signals. The arrows indicate relevant upgoing reflection events.

4.3 | Results for Common-Receiver Gathers

With the evidence of the results obtained so far for DAS VSPs from a single source, the analysis was then extended to common-receiver data, that is, the data of a fixed receiver obtained with a plurality of sources at the surface. The analysis confirms that the dual-signal processing method is robust. Notwithstanding the low number of correlated records (six) stacked for each shot position, the analysis shows that the signal can be appreciated in the common-receiver data.

The source acquisition layout used in this 3D experiment consists of several line branches of different extensions (Figure 2). We investigate the results obtained with receivers at different reference depths in well R-3 and sources from line 200. Then we analyse the data measured at large offsets, up to the maximum offset of approximately 1.1 km from lines 400 and 600 (Figure 2). The source interval in these lines is 20, 40 and 80 m, respectively.

Figure 14 shows the results obtained with the source points of line 200 (Figure 2) at well depths 303, 564 and 846 m. We may observe that in some gathers the direct arrivals are better interpretable in the dual signals shown in column (b) than in the native total field shown in column (a). This effect is evident in particular for the data calculated at depth 846 m. The models of the incident rays at the receivers in the well R-3 are shown in Figures 15a and 15b for direct waves and waves reflected from the H6 horizon, that is, the top of the Menderes formation (red layer), respectively. The incidence angles are quite different at the different depths but also for direct and reflected arrivals, characterized by asymmetrical trends caused by the up-dip distribution of the reflection points on Menderes. We use the incidence angles a_i relative to the DAS axis to calculate the $\cos^2 a_i$ theoretical DAS sensitivity to strain induced by P-waves for direct (Figure 16a) and reflected arrivals (Figure 16b). These curves are modelled as an indicative reference for the source–receiver sensitivity. The field data are bandpass filtered 4-8-110-140 Hz and the analysis does not include gauge length effects in the DAS signals. Figure 17a,b shows the RMS amplitude calculated in a narrow time window centred around the direct arrivals, for (a) the native DAS signal and (b) the calculated dual DAS signal. In each plot, the curves of the common-receiver data are presented for each VP in line 200 and displayed by relative amplitude, maintaining the scales between the values calculated for the different receiver depths. Apart from common variations in the DAS signals consistent probably with variations of the recording response at different VP positions, the trends indicatively agree with the sensitivity curves of Figure 16a, scaled at different relative amplitudes because of spherical divergence and attenuation in the field data.

In Figure 17b, we compare the real amplitude responses of the calculated dual DAS signals, which are similar to the native DAS responses of Figure 17a, apart from an inversion of the amplitudes calculated at 564 and 846 m depth. This difference of amplitude

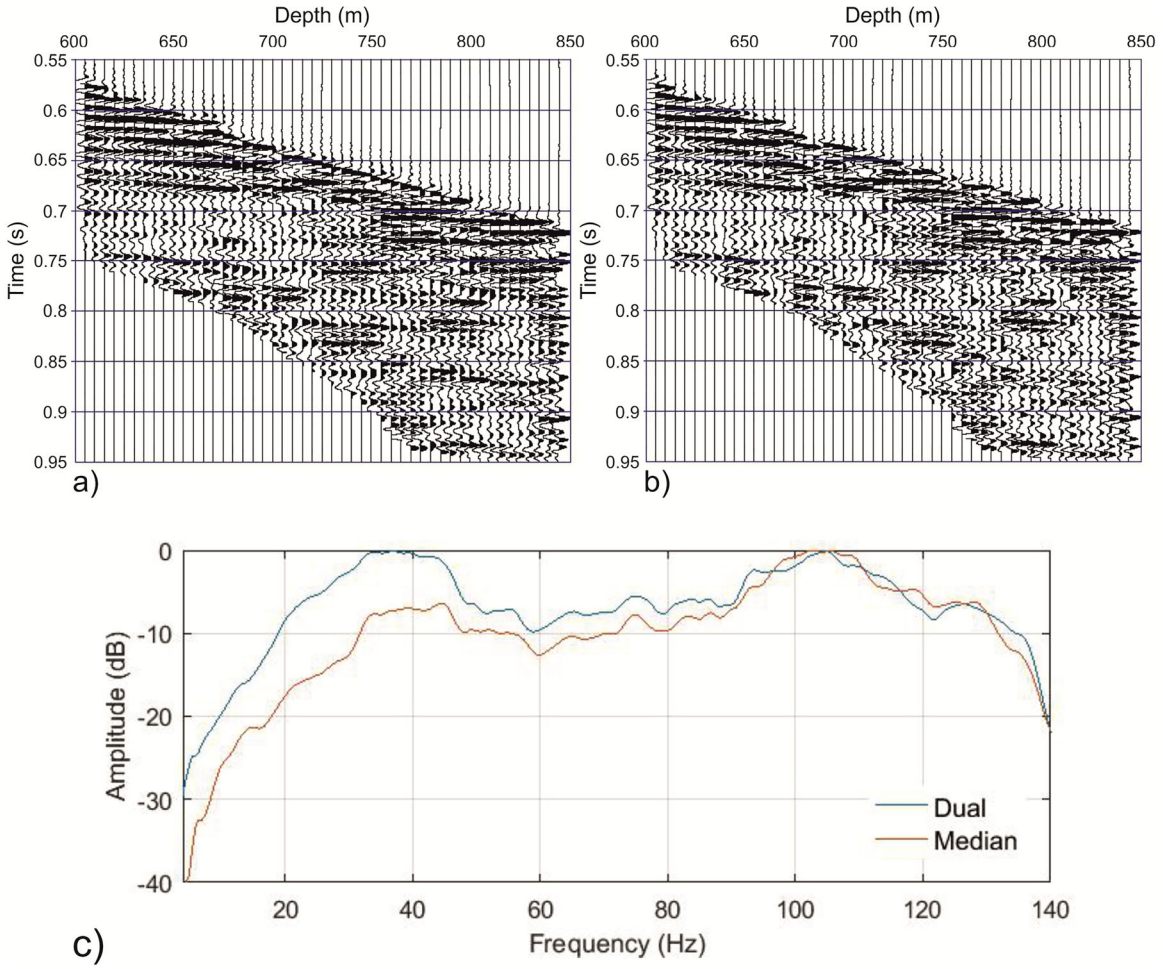

Figure 13 | Panels (a) and (b) show the upgoing signals of Figure 12a and 12b, respectively. The signals are aligned to two-way-time by adding the direct-arrival traveltimes. The traces are extracted at every 5 m depth. A mute is applied to the data before the corridor stack. The two stacked time traces obtained for (a) and (b) are not shown. Panel (c) shows the amplitude spectra in the Fourier frequency domain (dB) of the corridor-stack traces obtained by the dual and median-filter wavefield separation. A smoothing in frequency is applied to the spectra using a 15-Hz window.

is interpreted as probably being due to the different interference of the direct and reflected arrivals.

This effect is clearly observable in Figure 14 at 846 m depth and, in our opinion, is one of the reasons to use the dual-signal processing method for a refined treatment of the DAS data.

Figure 18 shows the total field and the DW and UP results obtained with the data of Figure 14. Although in this combination, calculated with an averaged constant coefficient α, the calculated UP (column (c)) results show residuals of the DW fields (column (b)), these results provide new insight for the interpretation of the wavefields. So far, the results have been obtained with a bulk combination coefficient. A refined analysis of results obtainable using a variable combination coefficient α is a key aspect for motivations evaluated in the discussion section. Figure 19 shows the comparison of common-source and common-receiver gathers to highlight the interpretation of the UP and DW events, which are verified using the provisional arrival times calculated by raytracing using the 3D VSP velocity model. Figure 19a shows the UP VSP obtained in the proximity of the well at VP 221. The maximum displayed VSP depth is 564 m (marked by a red line), to match the depth of the UP common-receiver gather shown in Figure 19b, where the position of VP 221 is marked by the red line. Yellow dots show the interpreted events as residuals of DW arrivals interfering with UP waves, as well as UP reflections in both (a) and (b). This analysis helps to investigate and confirm the nature of the interpreted signals. The depth interval in panel (a) is subsampled and shown with VSP traces every 5 m, for display purposes. Figure 19c shows the details of the data after bandpass filtering 18–84 Hz. A short time window is used for wavelet deconvolution to mitigate undesired offset effects in Figure 18c. The event marked by M is interpreted as the UP reflection from the Menderes reservoir formation, which is in agreement with the modelling results. The velocity model used to calculate the expected formation reflection times was obtained by traveltime inversion of the direct arrivals (Vesnaver and Böhm 2000; Böhm et al. 2015), picked in the DAS VSP traces using the conventional VSP method. For the calculation of the formation reflection times, we use a 2D velocity slice extracted from the 3D DAS VSP model, which is shown in section C of Figure 20, where the 2D sections denoted as A, B and C in the map are extracted from the 3D tomographic model calculated by 3D inversion of the DAS VSP first arrivals.

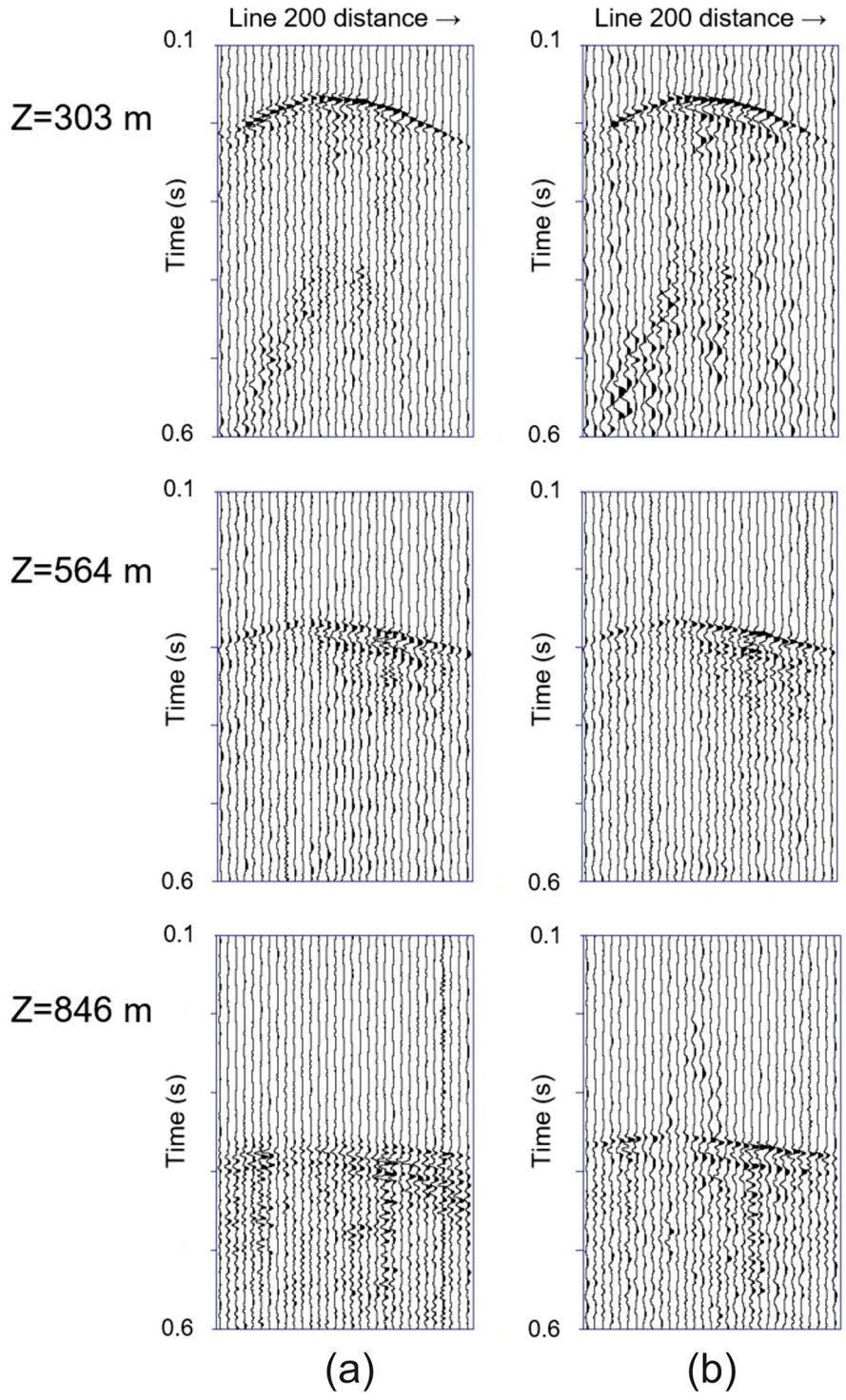

Figure 14 | Common-receiver gathers obtained using the VPs along source line 200 in Figure 2. We compare the (a) native total field and (b) the calculated dual fields obtained at receiver depths 303, 564 and 846 m in well R-3, respectively.

These results confirm that the dual-signal method can be effectively used in 3D configurations, that is, with a 3D array of the sources around the wells, to provide data for subsequent imaging and to better interpret wavefield characteristics at depth in the wells. This aspect is even more important in a time-lapse perspective.

5 | Dual DAS Signals for 3D VSP

In the early part of this work, the impact of dual-signal processing was verified for near-offset and medium-offset VSPs. In the following, we investigate aspects related to the quality of the signal recorded with wide offsets usable for 3D VSP purposes and

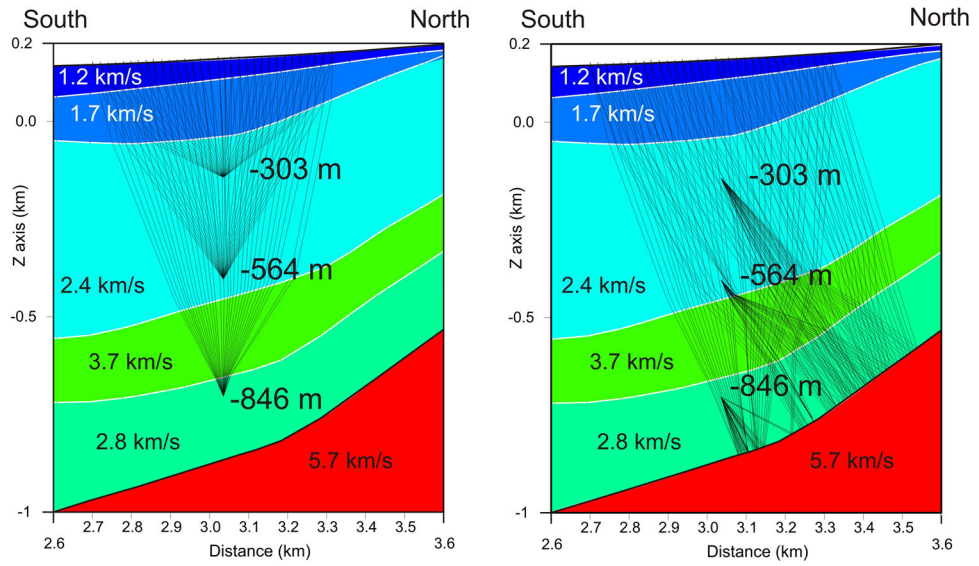

Figure 15 | (a) Direct and (b) reflected rays from the top horizon of the Menderes formation (H6), recorded at depths 303, 564 and 846 m in well R-3. The rays are calculated in the 3D model. The panels show the rays' 2D projections.

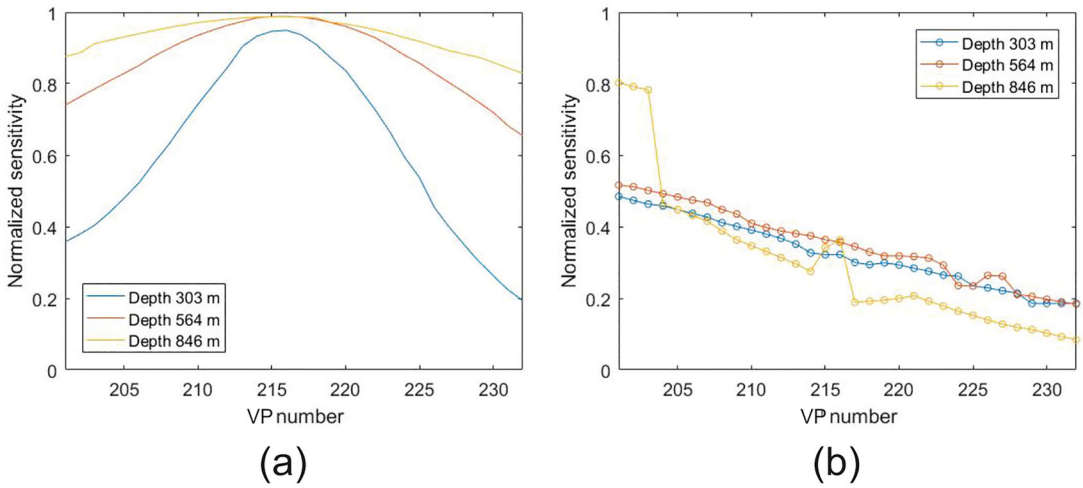

Figure 16 | Normalized DAS sensitivity calculated using the modelled incidence angles relative to the DAS axis of (a) the direct P-wave rays and (b) the H6 reflections at the receiver depths 303, 564 and 846 m. The horizontal scale is the VP number along line 200.

possibly for improved signal analysis after wavefield separation, so far obtained by averaged bulk calibration coefficients.

5.1 | Improved Direct-Arrival's Recognition by Dual Signals

One of the advantages of the dual-processing method is the improvement of the direct arrivals. This evident advantage of dual-signal processing is shown in Figure 21, where traces are displayed every 5 m. The direct arrival in the native common-source VSP is a superposition of the direct and reflection signals. The same effect occurs in the corresponding dual signal, but with UP reflections of opposite polarity. The sum of these signals (to obtain DW) removes the UP reflections, and the direct arrival is clearer.

5.2 | Use of Wide-Offset Signals

The application of dual-signal DAS processing for 3D VSP purposes depends on the capability to obtain near- and far-offset native data and combination results of suitable quality to allow effective interpretation and processing of DW and UP events.

Wide-offset common-receiver gathers, with maximum offset 1.1 km from well R-3, are analysed for this purpose in Figure 22, where the signals of lines 400 and 600 (Figure 2) are shown. The distances of the VPs in these lines are different (Figure 2).

These signals are recorded at 904 m depth in observation well R-3. Plotted using the different line orientations of the recorded data, the wider-offset traces of line 400 are displayed on the right side of the panels (Figure 22a), while the wider-offset traces of line 600 are displayed on the left side of the panels in Figure

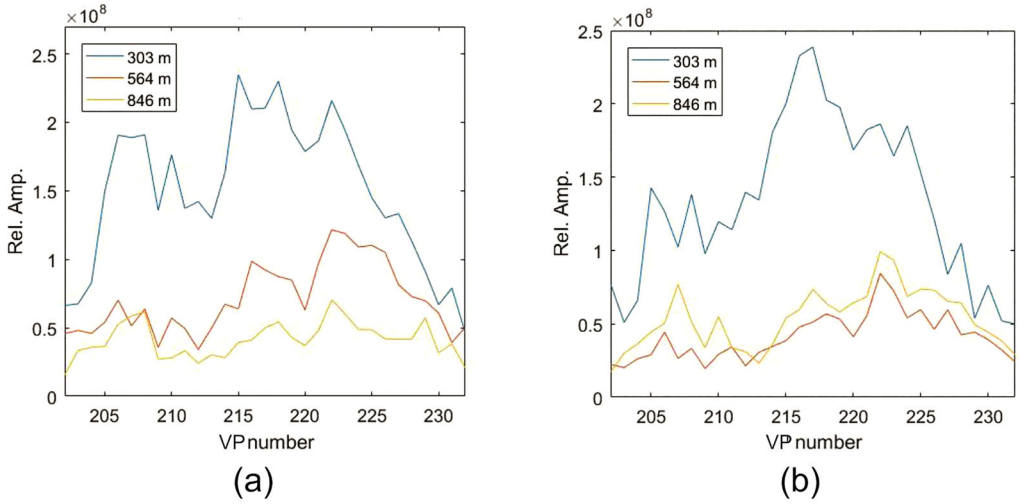

Figure 17 | Relative RMS amplitude of the real signals calculated in a short window around the direct arrivals in the common-receiver gathers recorded at the depths 303, 564 and 846 m. The figures show the curves of the (a) native DAS signal and (b) calculated dual signal. The horizontal scale is the VP number along line 200.

22b. The data are bandpass filtered to remove frequencies below 30 Hz. These data were recorded with the VPs along the main road. The analysis of noise components at lower frequencies is ongoing. We expect that these signals to have low and moderate DAS sensitivity variations for direct and reflected from Menderes (H6) signals, respectively. As an example, the receiver incidence angles relative to the DAS axis calculated using the 3D velocity model are shown in Figure 23. In the total field of line 600 shown in column (b) of Figure 22, three interpreted events are indicated by arrows. Gaining from the comparison of the total with the DW and UP signals, we interpret in the DW panel the DW signals, that is, the direct one (black arrow) is followed by a DWmultiple indicated by the green arrow. We interpret an UP signal, indicated by the bold red arrow in the UP panel, and the dashed arrow indicates the location of the removed direct arrival (not shown in the figure). In our evaluation, this example confirms that the dual field processing method provides separated data for improved interpretation of short- and medium-offset signals without direct-arrival picking and processing. The direct interpretation of these events in the wider offset traces of these fields and dual gathers before multichannel VSP processing seems focused on weaker signals. Obviously, these results have to be considered in the context of this survey, where six correlated records obtained using vibrator sweeps of 15 s were stacked at each VP. It is well known that, when achievable using a higher number of stacks, such as 24 or more, it significantly improves the SNR of the correlated DAS data, as shown in the QC tests.

5.3 | Variable Combination Coefficients

Another relevant aspect not only for 3D DAS VSP but also for single-offset DAS VSPs, as in the benchmark examples of Figure 10, is the calibration of variable combination coefficients. Figure 24 shows the estimated coefficients and their trend. The coefficients are calculated at the different depths by the ratio of the RMS values of the native and dual DAS signals in short time windows around the direct arrivals steered by the approximated curve of the first breaks (Poletto et al. 2016). The variations are related to local velocity variations in non-uniform models, changing with depth and offset, as well as signal interferences. This aspect is even more important for the 3D case. The wavefield separation is obtained from pairs of native and dual wave data. The latter is determined, apart from boundary details, from the well-defined processing of the native signal. Details may concern the choice of the integration verse and adopted compensation approach, the choice of the integration intervals to avoid noisy zones, and the possible tapering of the data to smooth abrupt side-edge conditions. Conversely, wavefield separation depends on the calibration of the coefficient α, which may be used to focus different types of waves, that is, signal or coherent noises with different progressive or regressive propagation velocities. This effect also concerns the propagation of waves in layers with different velocities. Apart from the benchmarking example of Figure 10, the wavefield separation of the DAS VSP data shown in the previous common-source and common-receiver examples was obtained using only one constant combination coefficient for the whole dataset. This means that using only one average α value to provide results can be used to characterize the VSP wavefields. Trace-by-trace tuning of the variable coefficient α based on the analysis of the signal RMS amplitude in a window centred around direct arrivals (NB: this is not detailed picking of the direct arrivals) was successfully demonstrated for DAS VSPs by Poletto et al. (2016), showing that variable calibration improves the dual DAS separation results for near-offset DAS VSP in non-uniform formations. However, with multi-offset data, we have to evaluate the target of the calibration strategy. This may improve separation results. For example, in Figure 14, the dual signal (b) at depth 846 m is better than the native signal (a) at the same depth. If we use (a) as the reference signal for calibration, the result is to weaken the direct arrival energy in (b) after scaling. The choice of the signal type and interval for the analysis window in the offset traces is therefore a key aspect for optimization of dual-signal analysis and processing. The analysis is related to the variable slowness of the wavefields. Figure 25 shows the results obtained with the data of line 400 at the reference receiver depth of 904 m.

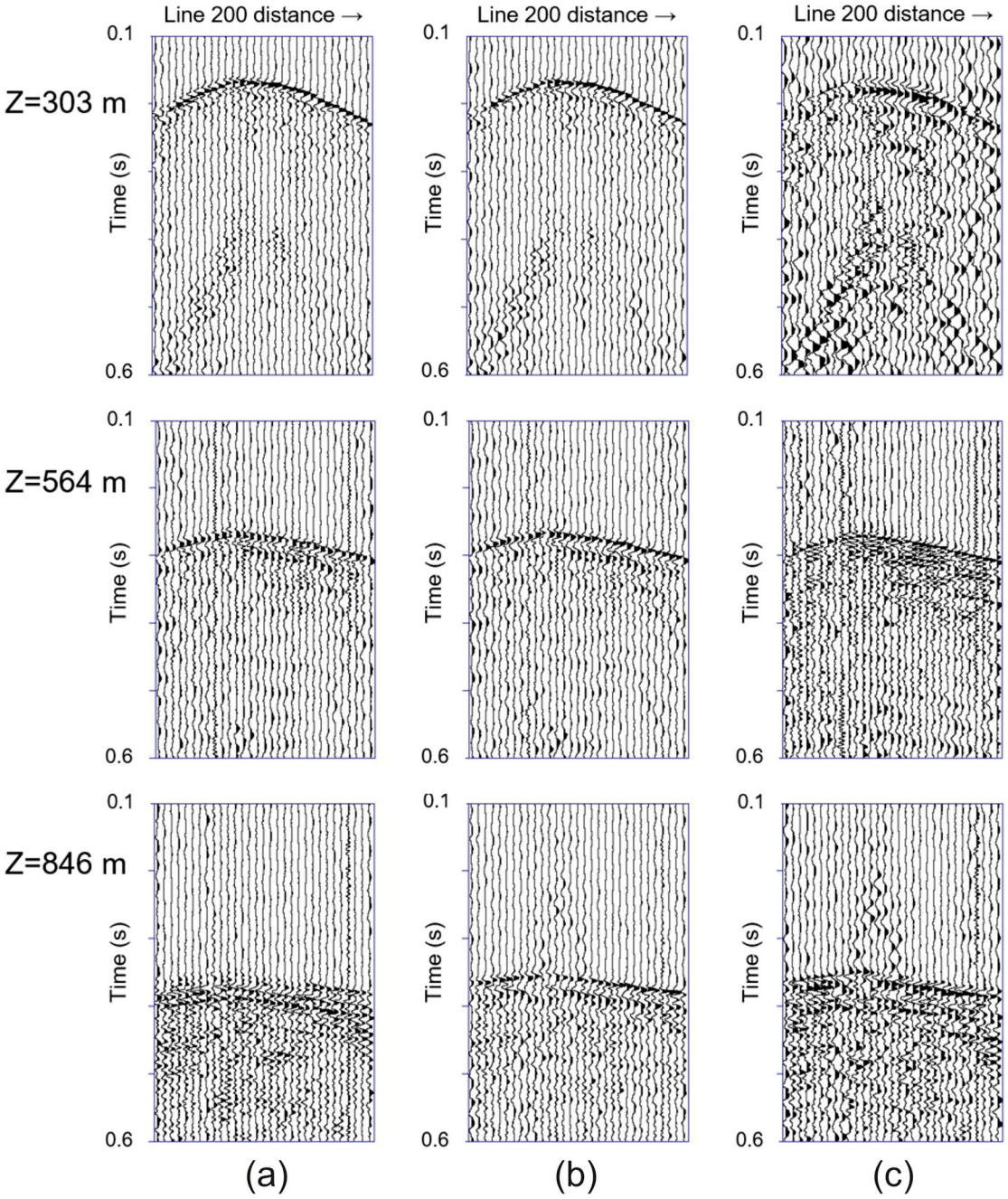

Figure 18 | Common-receiver gathers obtained using the vibration points of the source line 200 in Figure 2. We compare (a) the native total fields and the calculated (b) downgoing and (c) upgoing fields obtained at receiver depths 303, 564 and 846 m in well R-3.

Figure 25a shows the variable scaling coefficient estimated by the ratio of the native/dual signals' RMS amplitudes in a suitable window approximately centred around arrivals. The higher slowness (α) values correspond to the dipper slopes in short portions of the individual VSP versus depth centred around 904 m depth for the different contiguous VPs of line 400 (Figure 25b). A deeper signal analysis aimed at better understanding the involved wavefields would require a more detailed knowledge of the complex 3D seismic model (Figure 1), which is beyond the scope of this paper.

6 | Discussion

A main target of the variable-coefficient approach is to better tune and subtract the direct arrivals. This was done for sample tests. As observed above, the differences in the panels of Figures 14 and 18 are noticeable at a depth of 846 m. This difference in the signals means the UP wavefield separation is affected by direct and DW arrivals. We wonder if this effect is due to the different sensitivities of the dual signals to the wave incidence angle θ, where $\theta = 0$ means coaxial. For a linear cable, the DAS directional sensitivity

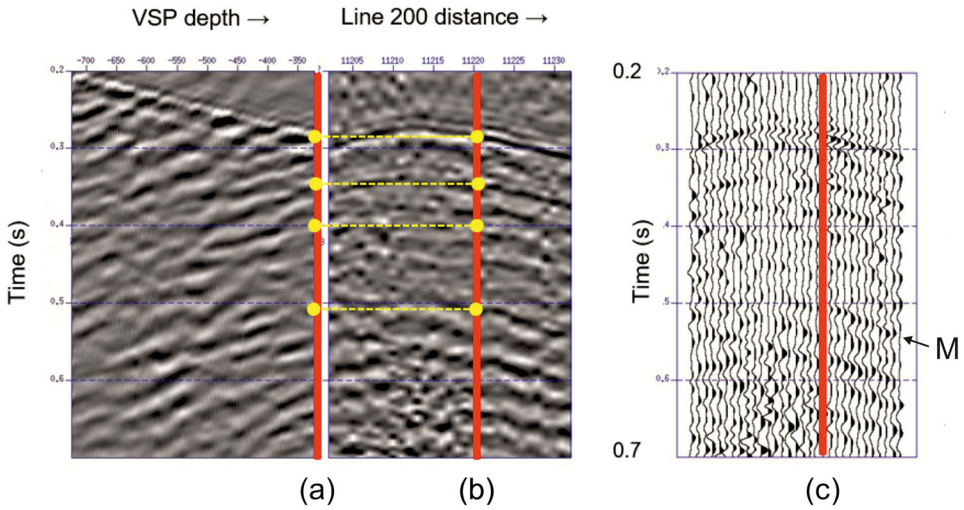

Figure 19 | (a) UP VSP of the VP 221, plotted with a maximum depth of 564 m. (b) Upgoing common-receiver VSP gather at depth 564 m. The red line marks the position of the VP 221. (c) Upgoing signal bandpass filtered between 18 and 84 Hz. The event marked by M is interpreted as the Menderes reflection. This interpretation in the common-receiver signal (c) is supported by the calculation of the synthetic traveltime arrivals using the provisional 3D velocity model shown in Figure 20 (section C).

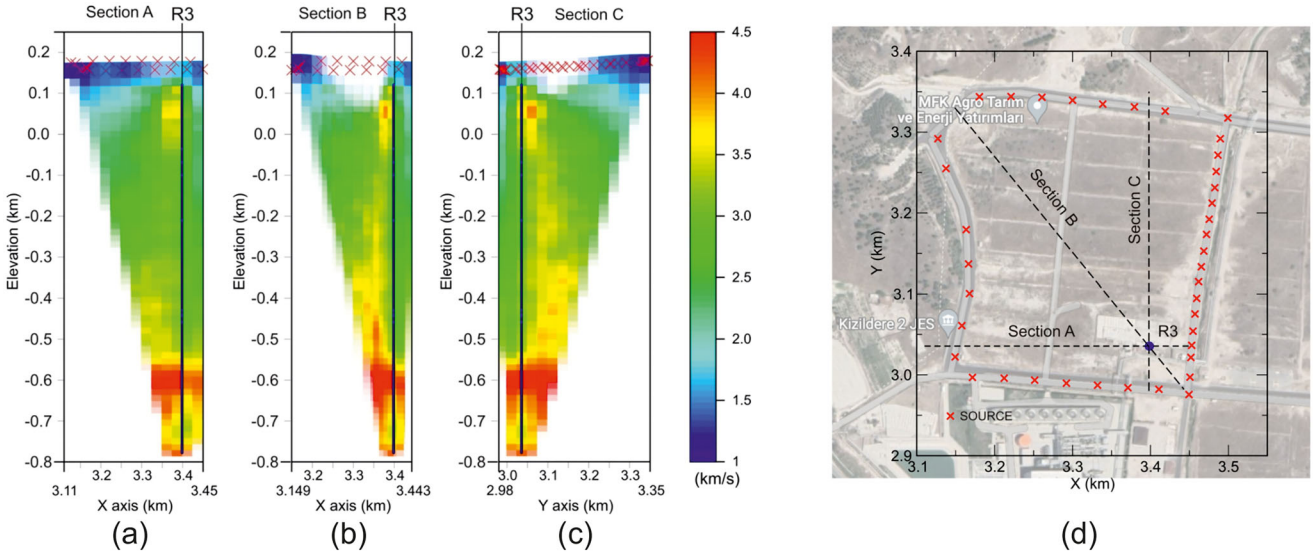

Figure 20 | Velocity sections obtained by traveltime inversion of direct arrivals of the 3D DAS VSP data. The 2D sections (a), (b) and (c) are extracted from the 3D model and are denoted as A, B and C in the map (d), respectively. The south-north section (c) was used for the calculation of the reflection traveltimes from selected layers.

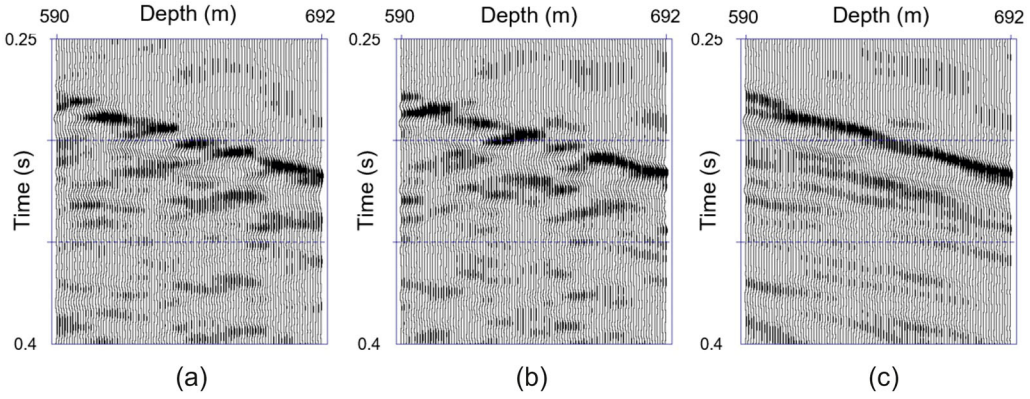

Figure 21 | (a) Native field, (b) dual field and c) downgoing field, where the direct arrival is better interpretable.

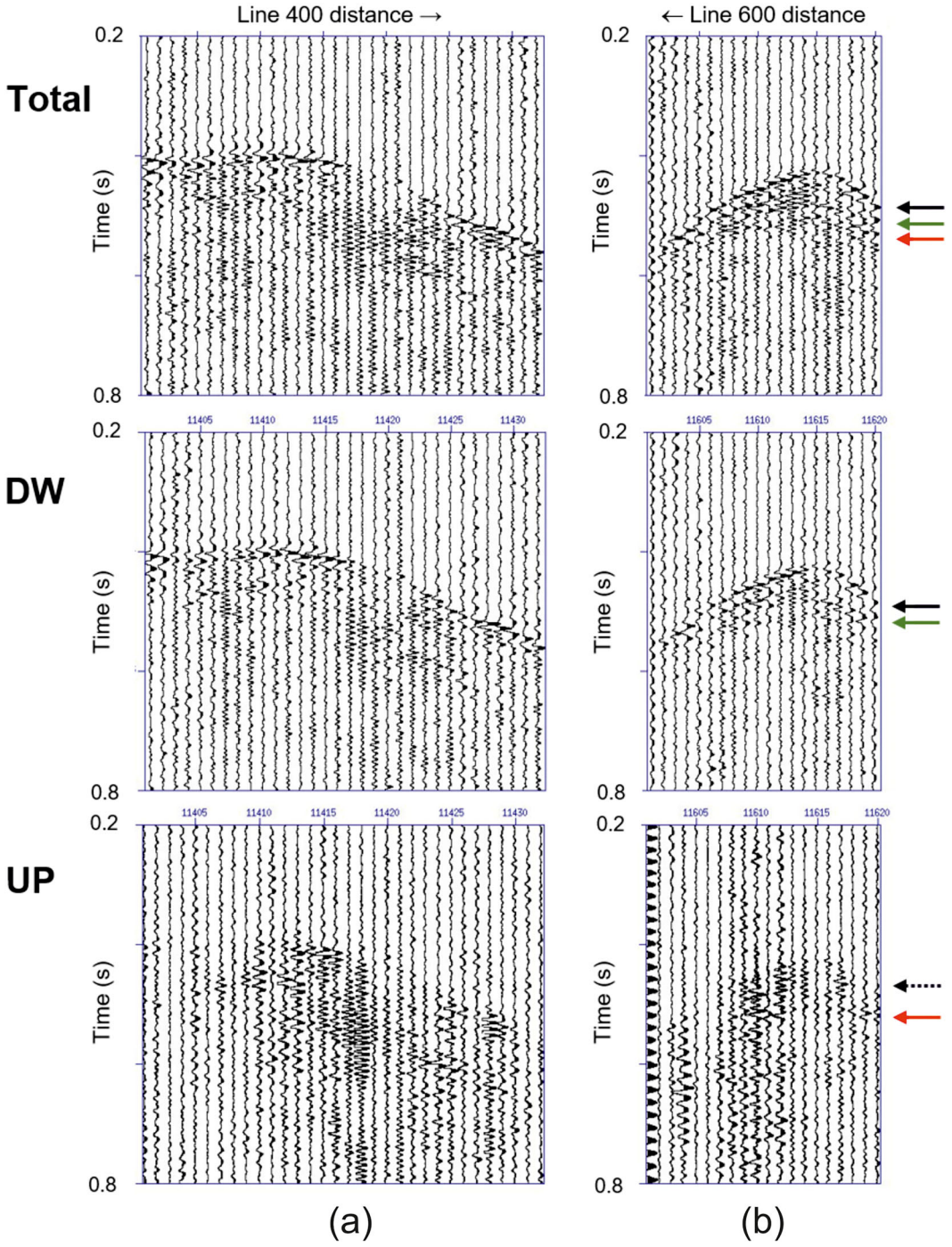

Figure 22 | Total and separated signals of common-receiver gathers recorded at depth 904 m with the source lines (a) 400 and (b) 600. These records contain traces with large offsets, up to approximately 1.1 km from well R-3.

response to P-waves is $\cos^2\theta$ (e.g., Mateeva et al. 2014; Kuvshinov 2016; Willis 2022), while the theoretical directional sensitivity of a geophone velocity transducer is $\cos\theta$. Moreover, the fibre optic gauge length of 10 m introduces another directional effect, which is stronger for axial waves. The gauge filter introduces a directional-sensitivity effect intermediate between those expected for borehole DAS and geophone data (Poletto and Miranda 2022).

Relevant advantages of the DAS dual-processing method are that it can provide quick data in the early-acquisition QC phase with usable reflection results to verify and promptly update the pre-survey reflectivity model. The results are supported by and compared to 3D VSP inversion results and show that the proposed method can be effectively used to improve the identification and analysis of wavefields, their interference in common-source and common-receiver gathers and to improve the detection of direct arrivals in recorded borehole signals. We think that this could be a great advantage coming from the dual-signal processing method for the processing of 3D DAS VSP datasets, in particular when the picking of the direct arrivals is problematic.

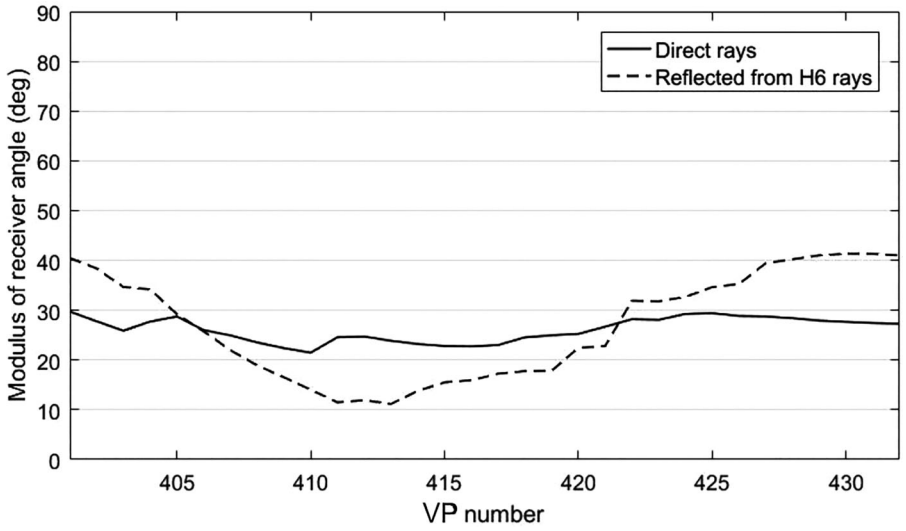

Figure 23 | Incidence angles at the receiver depth 904 m calculated in the 3D model for the VP positions along line 400. The solid and dashed lines represent the angles of the direct-arrival rays and rays reflected from H6, respectively.

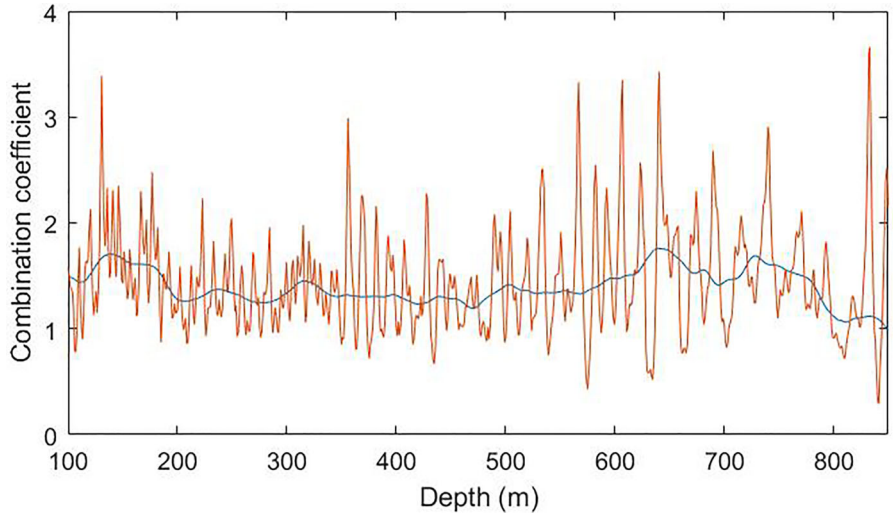

Figure 24 | Variable coefficients calculated from the field data to tune the wavefield separation by the combination of the native and the calculated dual signals of the QC DAS VSP. The curves plotted versus receiver depth show the scaling coefficients used for the combination (red line) and their smoothed profile (blue line).

An aspect of possible uncertainty in the signal interpretation is whether the signal variation is related to signal interference effects. These effects may occur when the direct arrival and reflections are superimposed, such as in Figure 14. We plan to investigate in future work these effects in the 3D DAS VSP dataset using signal-polarization analysis and ray tracing. This enhancement requires an improved 3D seismic model.

The proposed dual-signal processing method is not intended as a substitute for conventional VSP processing methods, but as a complementary approach to be integrated with the conventional analysis. The easy and quick calculation of the dual fields in the axial approximation provides new data from the native signal at a trace-to-trace level. In this case, we gain from the fine spatial sampling along a linear engineered high-sensitivity cable with receivers approximately at every 1-m depth. The 10-m gauge length acts as a filter that enables to reduce the density of the sampling to larger intervals for the dual-signal's calculation, with minor differences relative to the denser sampling.

7 | Conclusions

We presented the results of the dual-signal processing of common-source subsets from a 3D DAS VSP acquired in Turkey with a linear-high-sensitivity engineered borehole cable and a novel electric vibrator at the surface during the baseline campaign of a CO_2 injection monitoring project.

We demonstrated the adopted method to be robust for the processing of the signal signature and in the presence of noise. Moreover, it has proved effective with near-offset VSP data, as

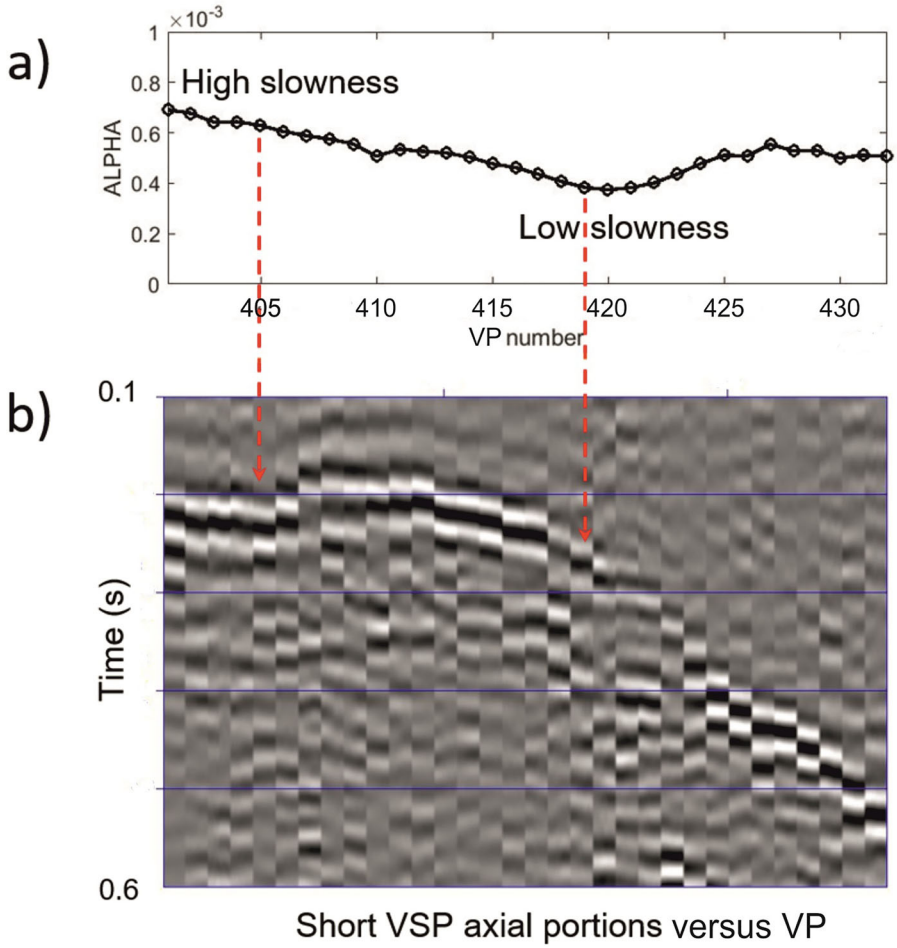

Figure 25 | (a) Calculated $\alpha = \alpha(z, SP)$ coefficients at depths 904 m for the shot points of line 400. (b) Short VSP intervals around depth 904 m, for the corresponding VPs positions along line 400.

well as with offset VSP data collected with 3D source positions, in some cases reaching large-offset limits, where horizontal signal moveouts may characterize problematic zones for wavefield recognition and processing with the dual-signal approach.

Our study demonstrated the consistency of the dual-wavefield results, which can be used to quickly improve the detection and interpretation of DW and UP fields at depth in the well. Benchmarking of the dual DAS VSP results with those of a conventional DAS VSP processing, we confirmed the robustness of the dual-signal method. The analysis of subsets extracted from the 3D dataset showed that the use of simple provisional dual-signal combination factors provides results of good/acceptable quality for wavefield interpretation.

The processing used to calculate the dual fields from the native DAS signal benefits from the dense and regular spatial sampling of the fibre-optic receiver array. The main advantage of the proposed method, which uses different physical quantities, similar to the conventional approach using hydrophone and geophone signals, is to easily provide quick results for early QC in a 3D DAS VSP, allowing prompt updating of the seismic model. Another relevant advantage is to provide improved data for first-arrival recognition within the 3D VSP dataset, to provide new data for the analysis of the signal interference, arrival times and waveforms. These aspects are of great importance from the perspective of 4D time-lapse applications. The optimization of variable combination coefficients for wavefield separation is a key step in non-uniform models. Next steps of the study will be the calibration of the combination parameters, with the support of the 3D DAS VSP model, obtained by processing the whole 3D dataset. The comparison of the dual VSP with surface seismic data and conventional processed DAS VSP wavefields in the complex reservoir will boost the investigation of the wavefields obtained with the dual-signal method. The potential of the method for future applications with shorter gauge lengths is envisaged to provide more detailed borehole images.

Acknowledgements

The authors would like to thank the numerous colleagues who contributed to the project. In particular, Andrea Schleifer for the acquisition supervision and field QC and Piero Corubolo for fruitful discussions in the comparison of dual-field DAS VSP and conventional results. The authors also thank Francesco Miranda for fruitful comments and discussions on DAS VSP signal processing and interpretation. The SUCCEED project is funded through the ACT programme (Accelerating CCS Technologies, Horizon 2020 Project No 294766). Financial contributions made by the Department for Business, Energy & Industrial Strategy UK (BEIS), the

Ministry of Economic Affairs and Climate Policy, the Netherlands, the Scientific and Technological Research Council of Turkey (TUBITAK), Orkuveita Reykjavíkur Iceland/Reykjavik Energy (OR) and the Istituto Nazionale di Oceanografia e di Geofisica Sperimentale (OGS), Italy, are gratefully acknowledged.

Open access publishing facilitated by Istituto Nazionale di Oceanografia e Geofisica Sperimentale, as part of the Wiley - CRUI-CARE agreement.

Data Availability Statement

The data that support the findings of this study are available from the corresponding author upon reasonable request.

References

Ali, S., F. Miranda, E. Spadavecchia, and R. Castaneda-Aguilar. 2021. "Processing of a Large Offshore 3DVSP DAS Survey in a Producing Well." In *First International Meeting for Applied Geoscience & Energy Expanded Abstracts*, 427–431. Society of Exploration Geophysicists.

Carcione, Böhm, G., J. M., D. Gei, S. Picotti, and A. Michelini. 2015. "Cross-Well Seismic and Electromagnetic Tomography for CO_2 Detection and Monitoring in a Saline Aquifer." *Journal of Petroleum Science and Engineering* 133: 245–257. https://doi.org/10.1016/j.petrol.2015.06.010.

Chalari, A., A. Stork, A. David, et al. 2023. "Monitoring High Temperature Geothermal Fields With Distributed Acoustic Sensing (DAS)." Paper presented at the SPE Workshop: In-Well Fibre-Optic Sensing - Applications for Field Development, Integrity and Optimisation, 22–23 February, The Hague, The Netherlands.

Correa, J., R. Isaenkov, S. Yavuz, et al. 2021. "Distributed Acoustic Sensing/Surface Orbital Vibrator: Rotary Seismic Sources with Fiber-Optic Sensing Facilitates Autonomous Permanent Reservoir Monitoring." *Geophysics* 86, no. 6: P61–P68. https://doi.org/10.1190/geo2020-0612.1.

Daley, T. M., D. E. Miller, K. Dodds, P. Cook, and B. M. Freifeld. 2016. "Field Testing of Modular Borehole Monitoring With Simultaneous Distributed Acoustic Sensing and Geophone Vertical Seismic Profiles at Citronelle, Alabama." *Geophysical Prospecting* 64: 1318–1334. https://doi.org/10.1111/1365-2478.12324.

Durucan, Ş., A. Korre, M. Parlaktuna, et al. 2021. "SUCCEED: A CO_2 Storage and Utilisation Project Aimed at Mitigating Against Greenhouse Gas Emissions from Geothermal Power Production." Paper presented at the 15th International Conference on Greenhouse Gas Control Technologies, GHGT-15, Abu Dhabi, 1–7.

Furre, A.-K., and O. Eiken. 2014. "Dual Sensor Streamer Technology Used in Sleipner CO_2 Injection Monitoring." *Geophysical Prospecting* 62: 1075–1088. https://doi.org/10.1111/1365-2478.12120.

Hardage, B. 1983. *Vertical Seismic Profiling: Part A: Principles*. Geophysical Press.

Janssen, M., A. Barnhoorn, D. Draganov, K. H. Wolf, and S. Durucan. 2021. "Seismic Velocity Characterisation of Geothermal Reservoir Rocks for CO_2 Storage Performance Assessment." *Applied Science* 11, no. 8: 3641. https://doi.org/10.3390/app11083641.

Kragh, E., and P. Christie. 2002. "Seismic Repeatability, Normalized RMS, and Predictability." *The Leading Edge* 21: 617–712. https://doi.org/10.1190/1.1497316.

Kuvshinov, B. N. 2016. "Interaction of Helically Wound Fibre-Optic Cables With Plane Seismic Waves." *Geophysical Prospecting* 64, no. 3: 671–688.

Loewenthal, D., and E. A. Robinson. 2000. "On Unified Dual Fields and Einstein Deconvolution." *Geophysics* 65, no. 1: 293–303. https://doi.org/10.1190/1.1444720.

Liborio, C., M. Fervari, M. Mariotti, A. Cerliani, F. Miranda, and M. Ferla. 2023. "An Integrated Quantitative Approach to Optimize Subsurface Reservoir Model With 3D DAS VSP." . In *7th EAGE Borehole Geophysics Workshop, Expanded Abstracts*, Milano, Italy, Paper P-51. European Association of Geoscientists & Engineers. https://doi.org/10.3997/2214-4609.2023101415.

Martuganova, E., M. Stiller, B. Norden, J. Henninges, and C. M. Krawczyk. 2022. "3D Deep Geothermal Reservoir Imaging With Wireline Distributed Acoustic Sensing in Two Boreholes." *Solid Earth* 13, no. 8: 1291–1307.

Mateeva, A., J. Lopez, H. Potters, et al. 2014. "Distributed Acoustic Sensing for Reservoir Monitoring with Vertical Seismic Profiling." *Geophysical Prospecting* 62: 679–692. https://doi.org/10.1111/1365-2478.12116.

Meneghini, F., F. Poletto, C. Bellezza, et al. 2024. "Feasibility Study and Results From a Baseline Multi-Tool Active Seismic Acquisition for CO_2 Monitoring at the Hellishei ð i Geothermal Field." *Sustainability* 1-23, no. 16: 7640. https://doi.org/10.3390/su16177640.

Parlaktuna, M., S. Durucan, B. Parlaktuna, et al. 2021. "Seismic Velocity Characterisation and Survey Design to Assess CO_2 Injection Performance at Kızıldere Geothermal Field." *Turkish Journal of Earth Science* 30, no. 9: Article 5. https://doi.org/10.3906/yer-2106-22. Available at: https://journals.tubitak.gov.tr/earth/vol30/iss9/5.

Poletto, F., D. Finfer, P. Corubolo, and B. Farina. 2016. "Dual Wavefields From Distributed Acoustic Sensing Measurements." *Geophysics* 81, no. 6: D585–D597. https://doi.org/10.1190/GEO2016-0073.1.

Poletto, F., M. Malusa, F. Miranda, and U. Tinivella. 2004. "Seismic-While-Drilling By Using Dual Sensors in Drill Strings." *Geophysics* 69, no. 5: 1261–1271. https://doi.org/10.1190/1.1801943.

Poletto, F., and F. Miranda. 2022. *Seismic While Drilling - Fundamentals of Drill-Bit Seismic for Exploration*, 2nd rev. ed. Elsevier.

Poletto, F., A. Schleifer, G. Böhm, et al. 2023. "Dual-Signal Processing of DAS-VSP Data of the Kizildere Geothermal Field." In *Seventh EAGE Borehole Geophysics Workshop, Expanded Abstracts*, 1–5. European Association of Geoscientists & Engineers. https://doi.org/10.3997/2214-4609.2023629019.

Sayed, A., S. Shujaat Ali, and R. R. Stewart. 2020. "Distributed Acoustic Sensing (DAS) to Velocity Transform and Its Benefits." Paper presented at the SEG International Exposition and Annual Meeting, Virtual, October 2020. Paper Number: SEG-2020-3424622. https://doi.org/10.1190/segam2020-3424622.1.

Simsek, S., N. Yıldırım, and A. Gungor. 2005. "Developmental and Environmental Effects of the Kızıldere Geothermal Power Project, Turkey." *Geothermics* 34: 239–256.

Soulas, S., G. Tubridy, S. Berry, et al. 2023. "The Rosemanowes DAS VSP Turkey Shoot Versus Geophones: A Quantitative Comparison." In *Seventh EAGE Borehole Geophysics Workshop, Expanded Abstracts*, 1–6. European Association of Geoscientists & Engineers. https://doi.org/10.3997/2214-4609.2023629002.

Vesnaver, A., and G. Böhm. 2000. "Staggered or Adapted Grids for Seismic Tomography?." *The Leading Edge* 19, no. 9: 944–950. https://doi.org/10.1190/1.1438762.

Willis, M. E. 2022. Distributed Acoustic Sensing for Seismic Measurements: What Geophysicists and Engineers Need to Know. Society of Exploration Geophysicists. Distinguished Instructor Series, No. 25. W.

Yu, G., H. Liu, Y. Zhang, et al. 2023. "Joint OBN and 3D DAS-VSP Data Acquisition and Processing in Offshore Abu Dhabi." Seventh EAGE Borehole Geophysics Workshop, 18-20 Sep 2023, Milan, Italy.

Zwartjes, P., A. Mateeva, D. Chalenski, Y. Duan, D. Kiyashchenko, and J. Lopez. 2018. "Frequent, Multi-Well, Stand-Alone 3D DAS VSP for Low-Cost Reservoir Monitoring in Deepwater." In *SEG International Exposition and 88th Annual Meeting* 4948–4952. Society of Exploration Geophysicists. https://doi.org/10.1190/segam2018-2997061.1.